A Study of the Mechanical Behavior of Particle Filled Elastomers

by

Lizabeth A. Montalvo

Submitted to the Department of Mechanical Engineering
in partial fulfillment of the requirements for the degree of

Bachelor of Science in Mechanical Engineering

at the

MASSACHUSETTS INSTITUTE OF TECHNOLOGY

June 1999

© Massachusetts Institute of Technology, 1999. All Rights Reserved.

Author .....
Department of Mechanical Engineering
May 21, 1999

Certified by .....
Professor M.C. Boyce
Department of Mechanical Engineering
Thesis Supervisor

Accepted by .....
Professor Derek Rowell
Chairman of the Undergraduate Thesis Committee
Department of Mechanical Engineering

MASSACHUSETTS INSTITUTE OF TECHNOLOGY
JUN 17 1999
LIBRARIES
ARCHIVES

A Study of the Mechanical Behavior of Particle Filled Elastomers

by

Lizabeth A. Montalvo

Submitted to the Department of Mechanical Engineering on May 21, 1999, in partial fulfillment of the requirements for the degree of Bachelor of Science in Mechanical Engineering

Abstract

The ability of elastomeric materials to undergo relatively large deformations in an elastic manner makes them the material of choice for a wide range of applications. Filler particles, such as carbon black, can be added to the elastomer to alter the mechanical behavior of the material when subjected to various loading conditions. The size, shape, and amount of filler particle added to the elastomer effects the mechanical properties. In this study, the micromechanics of filled elastomers are studied. We use the simple two dimensional axisymmetric Voronoi - Body Centered Cubic model, created by Socrate and Boyce [4], to aid in predicting the mechanical behavior of filled elastomers by means of a finite element program, ABAQUS. The effect of filler particles with 10%, 15%, and 20% volume fractions on the macroscopic axial stress vs. strain behavior and the microscopic strain and stretch of the matrix material are studied when the composite material is subjected to tensile and compressive uniaxial loading. The matrix material is taken to be chloroprene rubber. The study finds that the filler particles act to amplify the stretch incurred locally in the matrix material thus resulting in stiffer macroscopic behavior of the composite material as the volume fraction of filler particles is increased.

Thesis Supervisor: M.C. Boyce
Title: Associate Professor of the Mechanical Engineering Department

Table of Contents

1 Introduction 5
1.1 Background 5
1.2 Summary of Research 6
2 Development of the Micromechanical Model 7
2.1 Geometry - Voronoi - BCC Model 7
2.2 Matrix Constitutive Behavior 11
2.3 Cell Behavior 12
2.4 Description of Cases Simulated 14
3 Results and Discussion 16
3.1 Tension 16
3.1.1 Deformation 16
3.1.2 Stress vs. Strain Behavior 21
3.1.3 Tangent Modulus vs. Axial Strain 22
3.1.4 Tangent Modulus vs. Volume Fraction 23
3.1.5 Axial Strain 24
3.1.6 First Stretch Invariant 29
3.1.7 Axial Stress 33
3.2 Compression 37
3.2.1 Deformation 37
3.2.2 Stress vs. Strain Behavior 42
3.2.3 Tangent Modulus vs. Axial Strain 43
3.2.4 Tangent Modulus vs. Volume Fraction 45
3.2.5 Axial Strain 46
3.2.6 First Stetch Invariant 50
3.2.7 Axial Stress 54
4 Conclusions and Recommendations 58
4.1 Closing Remarks 58
4.2 Future Work 58
Appendix A Development of the Arruda and Boyce Eight Chain Model 59
Bibliography 60

List of Figures

Figure 2.1: Particles arranged on a regular BCC array 8
Figure 2.2: Construction of the three-dimensional V-BCC cell 8
Figure 2.3: The three - dimensional V-BCC cell 10
Figure 2.4: The axisymmetric V-BCC model 10
Figure 2.5: Unit Cell: 10%,15%, and 20% Vf of V-BCC and homopolymer 15
Figure 3.1: Uniaxial Tensile Deformation of V-BCC with 10% Vf 17
Figure 3.2: Uniaxial Tensile Deformation of V-BCC with 15% Vf 18
Figure 3.3: Uniaxial Tensile Deformation of V-BCC with 20% Vf 19
Figure 3.4: Uniaxial Tensile Deformation of Homopolymer 20
Figure 3.5: 100% Tension - V-BCC Model :Stress vs. Strain 21
Figure 3.6: Tangent Modulus vs. Strain - Voronoi - BCC Model. 23
Figure 3.7: Tangent Modulus versus Volume Fraction for Tensile Loading 24
Figure 3.8: Tensile Axial Strain of V-BCC with 10% Vf 26
Figure 3.9: Tensile Axial Strain of V-BCC with 15% Vf 27
Figure 3.10: Tensile Axial Strain of V-BCC with 20% Vf 28
Figure 3.11: First Strain Invariant of V-BCC in Tension with 10%Vf 30
Figure 3.12: First Strain Invariant of V-BCC in Tension with 15%Vf 31
Figure 3.13: First Strain Invariant of V-BCC in Tension with 20%Vf. 32
Figure 3.14: Tensile Axial Stress of V-BCC for 10% Vf: 34
Figure 3.15: Tensile Axial Stress of V-BCC for 15% Vf: 35
Figure 3.16: Tensile Axial Stress of V-BCC for 20% Vf: 36
Figure 3.17: Uniaxial Compressive Deformation of V-BCC with 10% Vf 38
Figure 3.18: Uniaxial Compressive Deformation of V-BCC with 15% Vf 39
Figure 3.19: Uniaxial Compressive Deformation of V-BCC with 20% Vf 40
Figure 3.20: Uniaxial Compressive Deformation of Homopolymer 41
Figure 3.21: 30% Compression - V-BCC Model :Stress vs. Strain 43
Figure 3.22: Tangent Modulus vs. Strain - Voronoi - BCC Model 44
Figure 3.23: Tangent Modulus versus Volume Fraction for Compressive Loading 45
Figure 3.24: Compressive Axial Strain of V-BCC with 10% Vf 47
Figure 3.25: Compressive Axial Strain of V-BCC with 15% Vf 48
Figure 3.26: Compressive Axial Strain of V-BCC with 20% Vf 49
Figure 3.27: First Strain Invariant of V-BCC in Compression with 10%Vf 51
Figure 3.28: First Strain Invariant of V-BCC in Compression with 15%Vf 52
Figure 3.29: First Strain Invariant of V-BCC in Compression with 20%Vf 53
Figure 3.30: Compressive Axial Stress of V-BCC for 10% Vf 55
Figure 3.31: Compressive Axial Stress of V-BCC for 15% Vf 56
Figure 3.32: Compressive Axial Stress of V-BCC for 20% Vf 57

1. Introduction

1.1 Background

Elastomeric materials are utilized in numerous commercial applications. The ability of elastomeric material to undergo relatively large deformations in an elastic manner makes them the material of choice for a wide range of applications. The stiffness of the elastomer is also easily adapted by the incorporation of filler particles which therefore enables tailoring of the mechanical properties. Filler particles, such as carbon black, can be added to the elastomer to alter the mechanical behavior of the material when subjected to various loading conditions. The mechanical behavior is affected by the type, shape, and amount of filler particle added to the elastomer. However, even though we have control over the properties of particle filled elastomers, further study is needed to develop models that will accurately predict the effects of particle material, shape and volume fraction on the mechanical behavior of the elastomer.

The mechanical behavior of a particle filled elastomer can be modeled using a representative volume element (RVE) of the composite material system, which is simply a geometric definition that embodies the essence of the microstructure under consideration [4]. The RVE model can then be implemented into a finite element modeling software by defining the proper model constraints and conditions. Bergstrom and Boyce [2] have studied the micromechanics of filled elastomers using three dimensional RVEs which consist of a random distribution of particles. A simpler approach is to use a RVE containing a single particle such as the axisymmetric Voronoi-BCC (V-BCC) model that has been developed by Socrate and Boyce [4] to study the micromechanics of toughened polycarbonate. The V-BCC model provides a realistic prediction of microscopic and macroscopic behavior of the material compared to other single particle axisymmetric models such as the Stacked

Hexagonal Array (SHA) [4]. The V-BCC model is also applicable for the study of deformation mechanisms in other heterogeneous systems and thus can be used to study particle filled elastomers [4].

1.2 Summary of Research

As previously mentioned, the V-BCC model is a reliable model for the study of the mechanical behavior of filled elastomers. Hence, the focus of this thesis it to study the mechanical behavior of a particle filled elastomer by means of the Voronoi-BCC RVE. The material properties of Chloroprene rubber were used for the study of the hyperelastic matrix material and a rigid particle such as carbon black was chosen to model the filler particle. The macroscopic response of the RVE as well as the local micromechanics of the matrix deformation are all studied for uniaxial tension and compression tests at particle volume fractions of 10%, 15%, and 20% for the Voronoi-BCC RVE of the filled elastomer. Macroscopic cell behavior is studied in terms of the stress-strain behavior and evolution in tangent modulus with strain for each volume fraction of filler. On the micromechanical level, the matrix deformation is studied by examining contours of matrix strain, stretch and stress in order to understand how the deformation of the matrix material is constrained by the particle thus producing the enhanced stiffness of particle-filled elastomers. Chapter 2, Development of the Micromechanical Model, elaborates on the development and constitutive models of the Voronoi-BCC model along with conditions and constraints that apply to the model due to the heterogeneous material combination. The results of the macroscopic and microscopic mechanical behavior are presented and discussed in Chapter 3. Finally, the last chapter summarizes the final remarks and further recommendations.

2. Development of the Micromechanical Model

Micromechanical models are used in order to understand the local mechanics and mechanisms governing the macroscopic deformation of heterogeneous materials. The basic features of the micromechanical model used to study the particle filled elastomers are geometry of the RVE, matrix constitutive behavior, and the cell behavior. Each feature is discussed along with a description of the cases examined for the filled elastomer.

2.1 Geometry - Voronoi-BCC Model

A well established approach to predicting the macroscopic mechanical behavior of a matrix material with inhomogenities relies on a spatially periodic representative volume element that deforms in a repetitive way, identical to its neighbors. The boundary conditions imposed on each RVE should ensure compatibility of the deformation field such that there is no material overlapping or separation at the boundary between two adjacent RVEs. The Voronoi Body Centered Cubic RVE, created by Socrate and Boyce, is a simple 2-D axisymmetric model which provides a realistic prediction of the mechanical behavior of heterogeneous materials [4].

The V-BCC axisymmetric model is adapted from the three dimensional V-BCC RVE. The 3D V-BCC model is created by arranging the filler particles of the heterogeneous material on a regular Body Centered Cubic (BCC) lattice as seen in Figure 2.1 from Socrate and Boyce [4]. The Voronoi tessellation procedure is used to build the RVE in three basic steps. First, we define three particles. P_0 is located at the center of the reference BCC cube, (P_1) are the eight particles at the vertices of the cube and (P_2) are the 6 particles at the centers of the adjacent BCC cubes. Particles (P_1) and (P_2) are all connected to P_0 by straight line segments. Second, each segment is bisected by a plane. Third, a truncated octahedron is formed as a body bounded by these planes. See Figure 2.2 for an illustration of the par-

ticles and the final octahedron shape. This truncated octahedron, also known as the Wigner-Seitz cell, is a highly symmetric polyhedron and completely fills space [4].

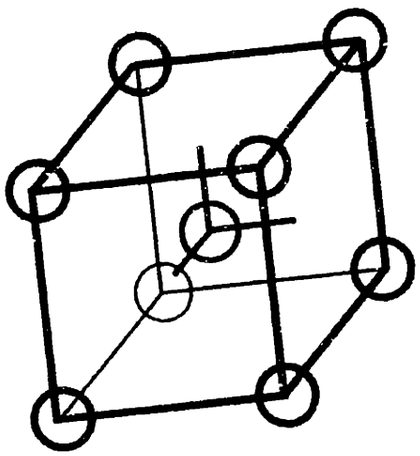

Figure 2.1: Particles arranged on a regular BCC array. Figure taken from Socrate and Boyce [4].

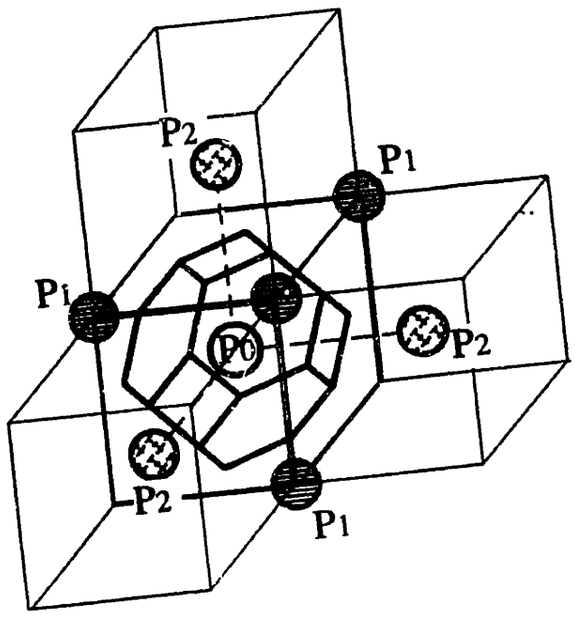

Figure 2.2: Construction of the three-dimensional V-BCC cell. Figure taken from Socrate and Boyce [4].

This three dimensional octahedron can be normalized by assuming unit distance between the staggered lattice planes so that the particles (P_1) are given by permutations of the cartesian coordinates $\{\pm 1, \pm 1, \pm 1\}$ with the origin at the center of the particle P_0 and axes aligned with the principal directions of the lattice (Figure 2.2). The section of material between z = 0 and z = 1 is constituted by cells centered at particles on the z = 0 plane and by an equal number of cells centered at particles on the z = 1 plane. Figure 2.3 illustrates the two types of cells, C_0 and C_1 centered on particles P_0 and P_1 respectively. To define the geometry of the cell mathematically, we consider a cross-section of the cells with plane $z=\xi$, and define the cross-sectional areas of cells C_0 and C_1 to be $A_0(\xi)$ and $A_1(\xi)$ respectively. The space filling properties of the RVE and symmetry conditions provide the following constraints:

$$A_0(\xi) + A_1(\xi) = \text{constant}, \tag{2.1}$$

$$A_0(\xi) = A_1(1-\xi), \tag{2.2}$$

which yield:

$$A_0(\xi) + A_0(1-\xi) = 2A_0|_{0.5} \tag{2.3}$$

where $A_0|_{0.5}$ is the cross-sectional area at the midplane of the cell (z = 0.5).

The truncated octahedron geometry provides the actual profile of cell cross-sectional area by

$$A_0(z) = 2(2.0 - (0.5 + z)^2) \tag{2.4}$$

$$\text{and } A_0(z) = 2(1.5 - z)^2. \tag{2.5}$$

However, since we are only studying the axisymmetric model, we reduce this RVE to an equivalent axisymmetric RVE as shown in Figure 2.4. This is the Voronoi-BCC model

based on the Voronoi tessellation of the BCC lattice which will be used to study the filled Chloroprene rubber.

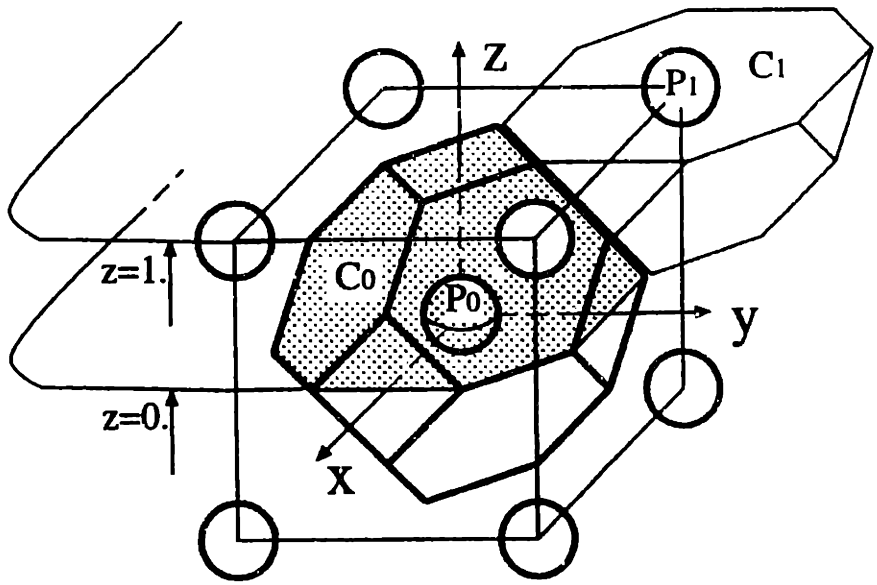

Figure 2.3: The two cells, C_1 and C_2, created from the three - dimensional V-BCC cell. Figure taken from Socrate and Boyce [4].

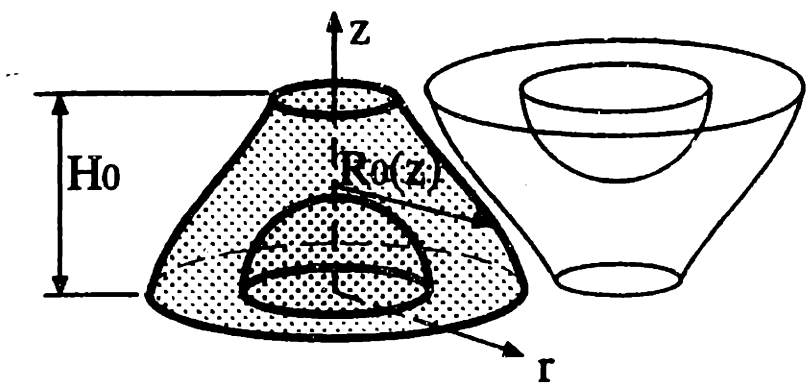

Figure 2.4: The axisymmetric V-BCC model. Figure taken from Socrate and Boyce [4].

2.2 Matrix Constitutive Behavior

The large stretch nonlinear elastic behavior of rubber materials has been found to be well-modeled using the constitutive model of Arruda and Boyce; therefore their model will be used to represent the behavior of the Chloroprene rubber matrix. The developed constitutive relation is based on an eight chain representation of the underlying macromolecular network structure of the rubber and the non-Gaussian behavior of the individual chains in the proposed network [1]. The eight chain model requires only two material parameters, an initial modulus and a limiting chain extensibility.

The Arruda-Boyce model yields the following stress-stretch relation for the eight chain model described in Appendix A.

$$\sigma_1 - \sigma_2 = \frac{nk\Theta}{3}\sqrt{N}L^{-1}\left[\frac{\lambda_{chain}}{\sqrt{N}}\right]\frac{(\lambda_1^2 - \lambda_2^2)}{\lambda_{chain}} \tag{2.6}$$

where σ_1 and σ_2 are principal stresses, n is the chain density, k is Boltzmann's constant, Θ is temperature, N is the number of rigid links in the chain, λ_{chain} is the chain stretch, λ_1 and λ_2 are the principal stretches and L^{-1} indicates the inverse Langevin function. The chain stretch is given by

$$\lambda_{chain} = \left(\frac{I_1}{3}\right)^{\frac{1}{2}} \tag{2.7}$$

where I_1 is the first stretch invariant $I_1=\lambda_1^2 + \lambda_1^2 + \lambda_1^2$. The eight chain model successfully accounts for the state of deformation dependence using a rubbery modulus and a locking stretch as its only two parameters, both of which can be determined from a single experiment [1].

The Arruda-Boyce material properties for Chloroprene rubber used for the V-BCC model were obtained from the Bergstrom and Boyce compression tests for Chloroprene rubber filled with 7% carbon black. [2].

2.3 Cell Behavior

As aforementioned, the objective of this study is to determine the effects of filled particles on the mechanical behavior of elastomers. We use the V-BCC axisymmetric RVE to model the matrix material with the inhomogenities. ABAQUS, a commercially available finite element program, is used to solve the boundary value problems posed on the V-BCC RVE. Figure 2.5 illustrates the homopolymer and the discretization of the unit cells for the V-BCC model for 10%, 15% and 20% volume fractions.

The constraints on the V-BCC cell behavior are governed by Equations (2.4) and (2.5) and the following determined relationships for size and displacement. The height of the V-BCC cell is H_0=1 and the external radius of the cell, R_0, varies with z by the following relationship:

$$R_0(z) = \sqrt{\frac{\overline{A_0(z)}}{\pi}}. \tag{2.8}$$

Due to axisymmetric loading and geometric compatibility of the deformation of the anti-symmetric cells, the radial displacement of the cell is defined by Socrate and Boyce [4] as

$$U_r(z) = (R_0(\xi) + U_r(\xi))^2 + (R_0(1-\xi) + U_r(1-\xi))^2 = 2(R_0|_{0.5} + U_r|_{0.5})^2 \tag{2.9}$$

where $U_r(\xi)$ is the radial displacement for a point at the outer radius of the cell, and $U_r|_{0.5}$

is the radial displacement of the point at the initial coordinates ($r = R_0$, $z = 0.5$). Symmetry also introduces a contraint on the profile of the axial displacement at the outer cell radius:

$$U_z(\xi) + U_z(1-\xi) = 2U_z|_{0.5} \tag{2.10}$$

where $U_z(\xi)$ is the axial displacement for a point at the outer radius of the cell and $U_z|_{0.5}$ is the axial displacement with the initial coordinates mentioned above.

In the V-BCC finite element model, the following boundary conditions have been adapted from Socrate and Boyce to meet the conditions on the filled elastomer [4]:

(1) nodes along the z-axis are, by definition, constrained to have zero radial displacement;

(2) nodes along the bottom surface of the cell are constrained to have zero axial displacement, as required by symmetry about the particle midplane ($z = 0$);

(3) nodes along the top plane ($z = 1.0$) of the cell are required to have equal axial displacement, $U_z|_{1.0}$;

(4) nodes along the particle edge are constrained to have zero radial and zero axial displacement in order to model a rigid filler particle.

(5) nodes along the outer radius of the cell are required to have radial and axial displacements which satisfy the conditions expressed through Equations (2.9) and (2.10). Note that due to symmetry of $U_z(\xi)$ about the midplane and constraint (2) of zero axial displacement for nodes along the bottom plane ($z = 0$), $U_z|_{0.5} = \frac{1}{2}U_z|_{1.0}$;

The axial component of the V-BCC macroscopic logarithmic strain can be expressed as:

$$E_z = \left(\frac{\ln H_0 + U_z|_{1.0}}{H_0}\right) = \ln(1 + U_z|_{1.0}), \tag{2.11}$$

where E_z is the axial strain and H_0 is the initial length of the V-BCC unit cell. The macroscopic axial stress component, Σ_z, is computed as the appropriate volume averages of the microscopic stress components:

$$\Sigma_z = \frac{1}{V} \int_{x \in V} \sigma_{zz}(x) dV. \tag{2.12}$$

This expression is evaluated in terms of the equivalent surface integrals along the outer boundary of the cells as mentioned by Socrate and Boyce [4].

A user-element subroutine was created by Socrate and Boyce to apply the traction boundary conditions to the V-BCC model in ABAQUS. For the displacement boundary conditions described in constraint (5) a "Multi Point Constraint (MPC)" user subroutine was imposed [4].

2.4 Description of Cases Simulated

The objective of this study is to observe the mechanical behavior of filled elastomers using the V-BCC model. Loading conditions on the cell was prescribed by applying a constant axial strain rate, $\dot{E}_z = 0.1s^{-1}$, for uniaxial tension and compression. The V-BCC model was adapted to 10%, 15%, and 20% filler particle volume fractions as seen in Figure 2.5. A homopolymer was also studied under identical loading conditions in order to monitor the effects of the filler particles on the composite (the carbon-black filled chloroprene) and compare to the unfilled elastomer, Chloroprene rubber. The user subroutines mentioned previously were implemented into the finite element simulations in order to monitor the macroscopic cell behavior. Both the macroscopic and local matrix mechanical behavior are presented by means of the matrix deformation, stress-strain behavior, first stretch invariant, and tangent modulus behavior.

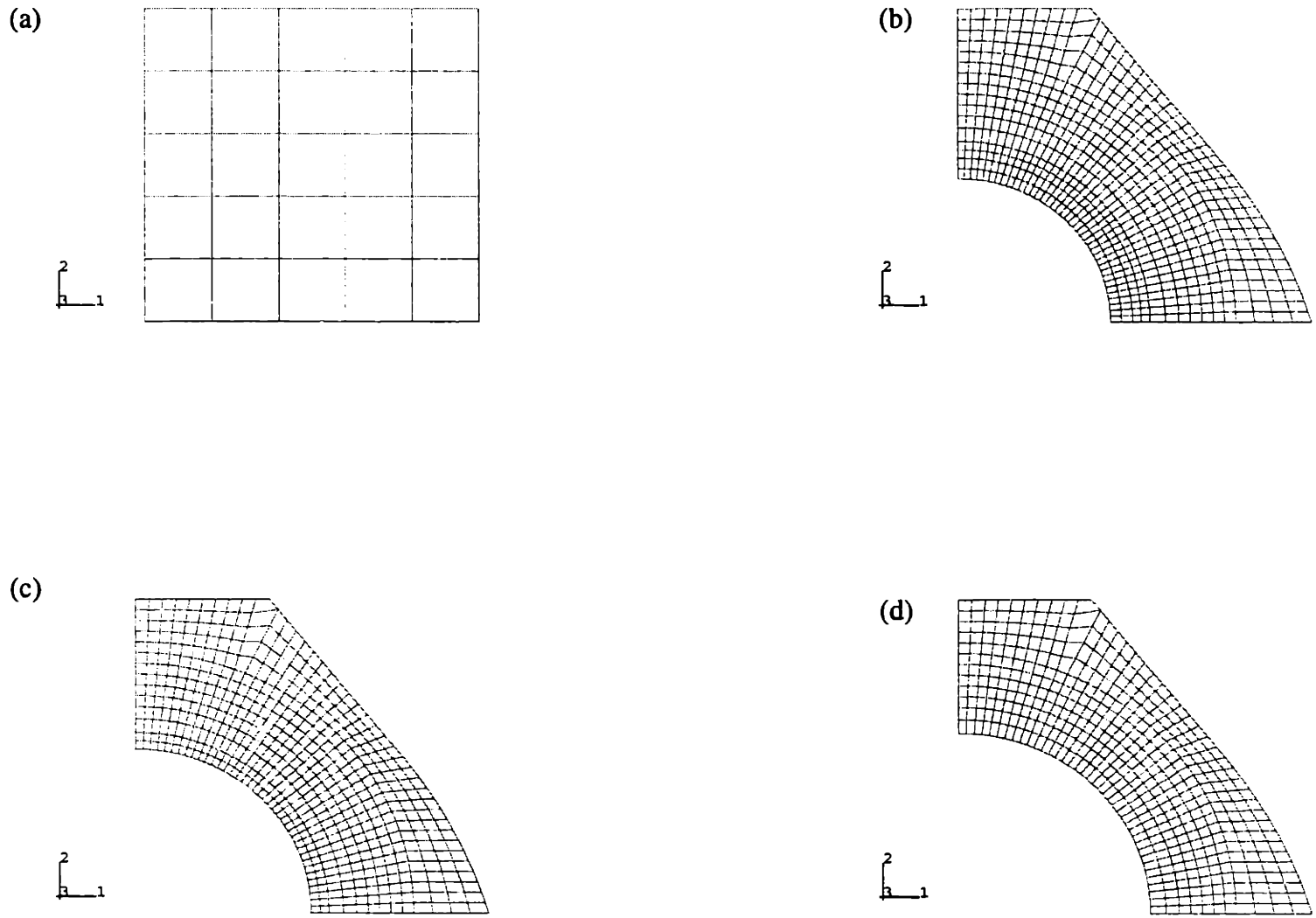

Figure 2.5: Unit Cell: (a) Homopolymer, (b) 10% Vf V-BCC, (c) 15% V-BCC, (d) 20% V-BCC

3. Results and Discussion

3.1 Tension

3.1.1 Deformation

The filled chloroprene rubber Voronoi-BCC RVE model was deformed to a final macroscopic axial strain of 0.7 at a constant strain rate of 0.1 s^{-1}. A logarithmic strain measure is used, $\varepsilon = \ln\left(\frac{h}{h_o}\right)$, where h is current length and h_0 is original length of the matrix.The final length of the filled elastomer is therefore twice its original height. Figures 3.1 through 3.4 illustrate the deformation of the elastomer where deformed meshes are depicted at strains of 0.0, 0.30, 0.50 and 0.70 for volume fractions of 10%, 15%, 20%, and the homopolymer respectively.

In Figure 3.1, the evolution in the deformation of the mesh with macroscopic axial strain illustrates how the matrix is deforming locally in order to accommodate the imposed strain. Since the matrix is perfectly adhered to the particle, there is little axial strain observed in the material laterally adjacent to the particle and the imposed strain is accommodated by amplified stretching of the material above the particle. This effect is discussed further later when contours of matrix strain and stress are examined.

Figures 3.2 and 3.3 depict similar responses as discussed for Figure 3.1 where the matrix deformation is even further amplified because of higher volume fraction of particles.

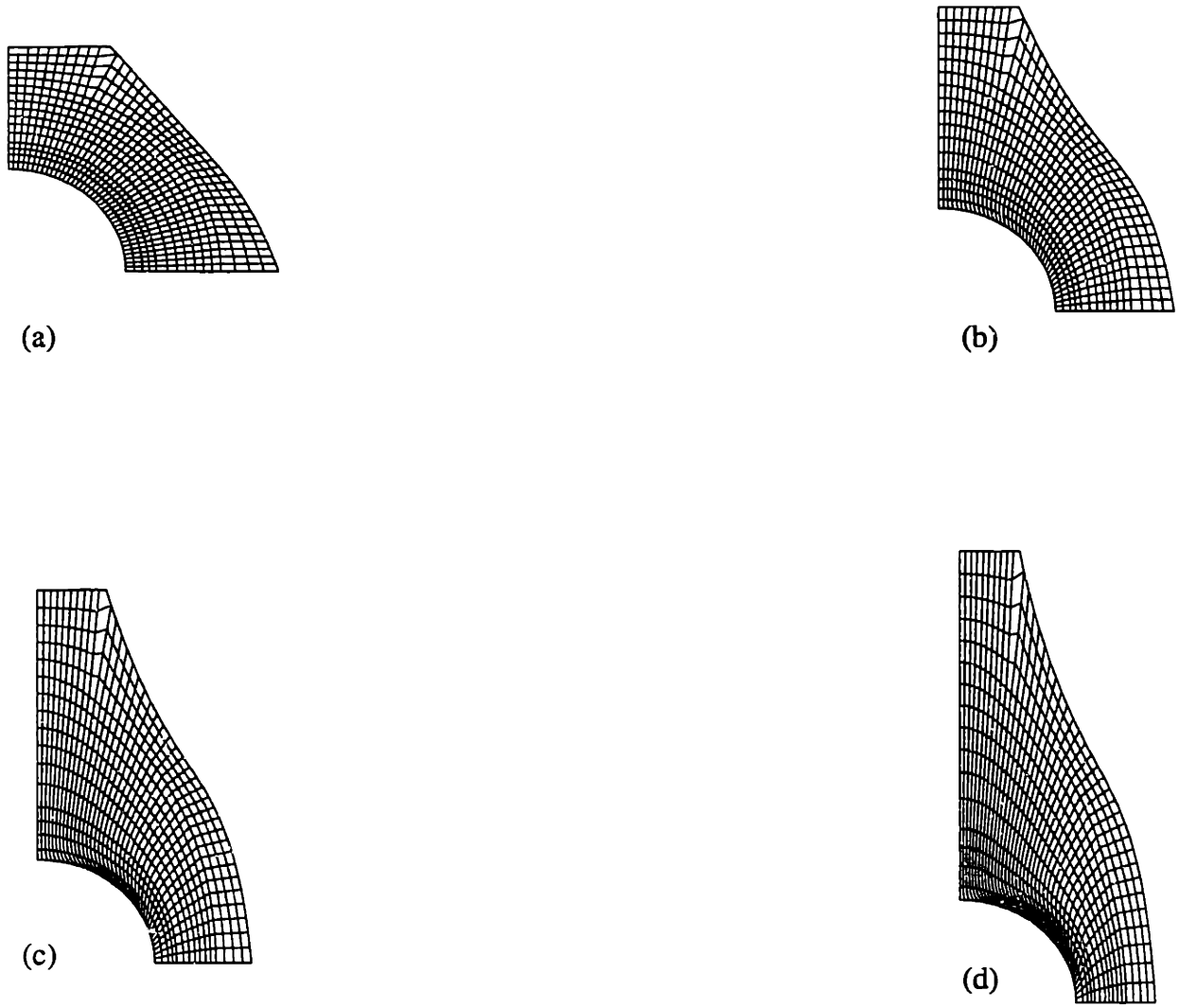

Figure 3.1: Uniaxial Tensile Deformation of V-BCC with 10% Vf: (a) E_z=0.0, (b) E_z=0.3, (c) E_z=0.5, (d) E_z=0.7

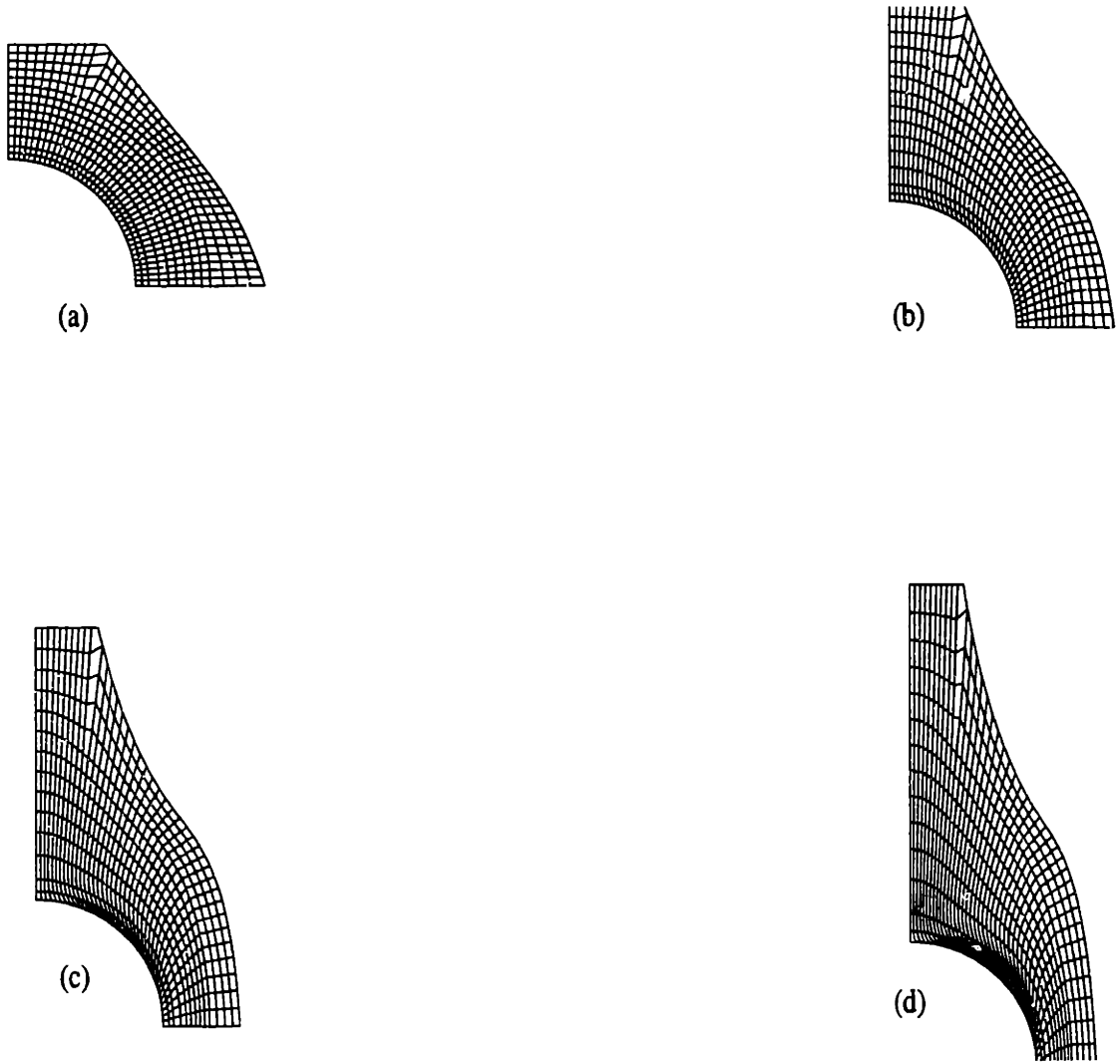

Figure 3.2: Uniaxial Tensile Deformation of V-BCC with 15% Vf: (a) E_z=0.0, (b) E_z=0.3, (c) E_z=0.5, (d) E_z=0.7

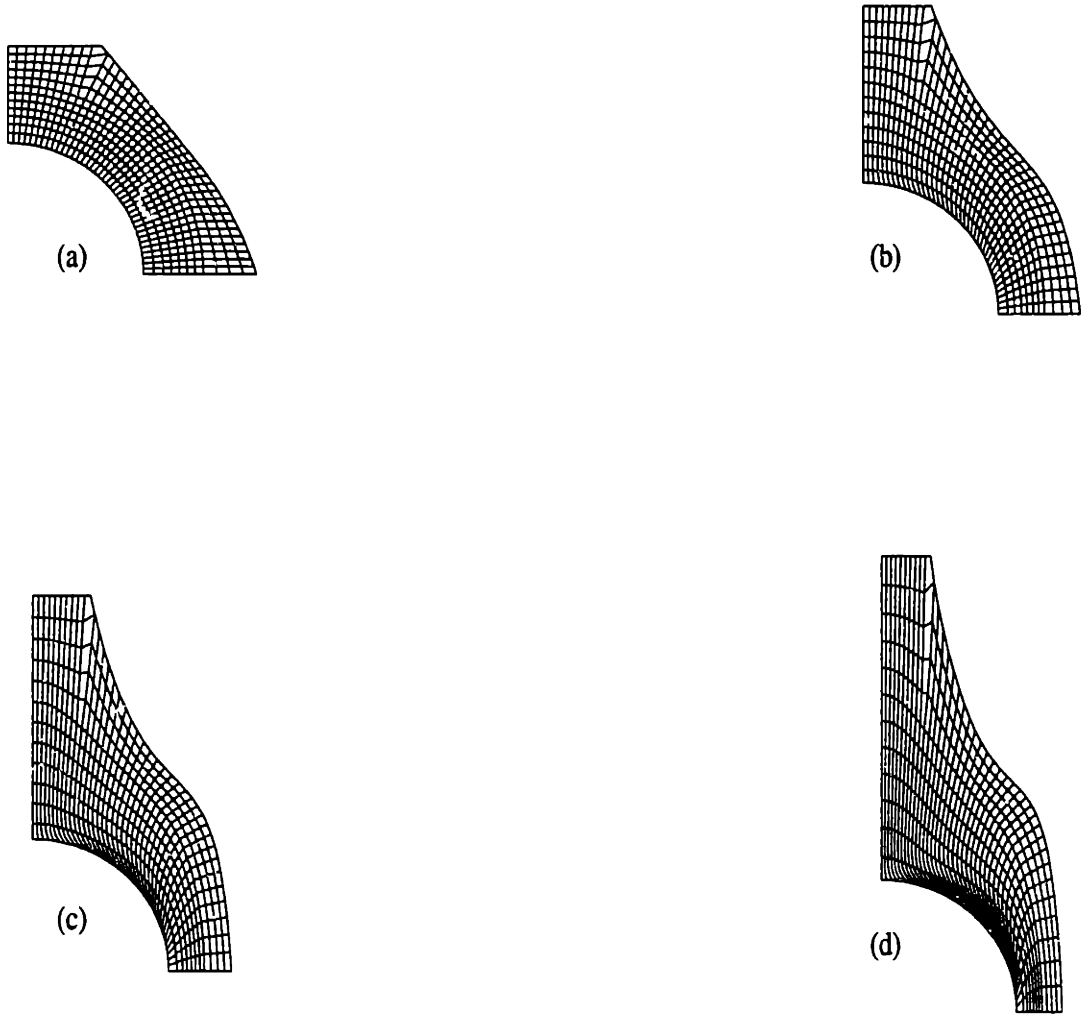

Figure 3.3: Uniaxial Tensile Deformation of V-BCC with 15% Vf: (a) E_z=0.0, (b) E_z=0.3, (c) E_z=0.5, (d) E_z=0.7

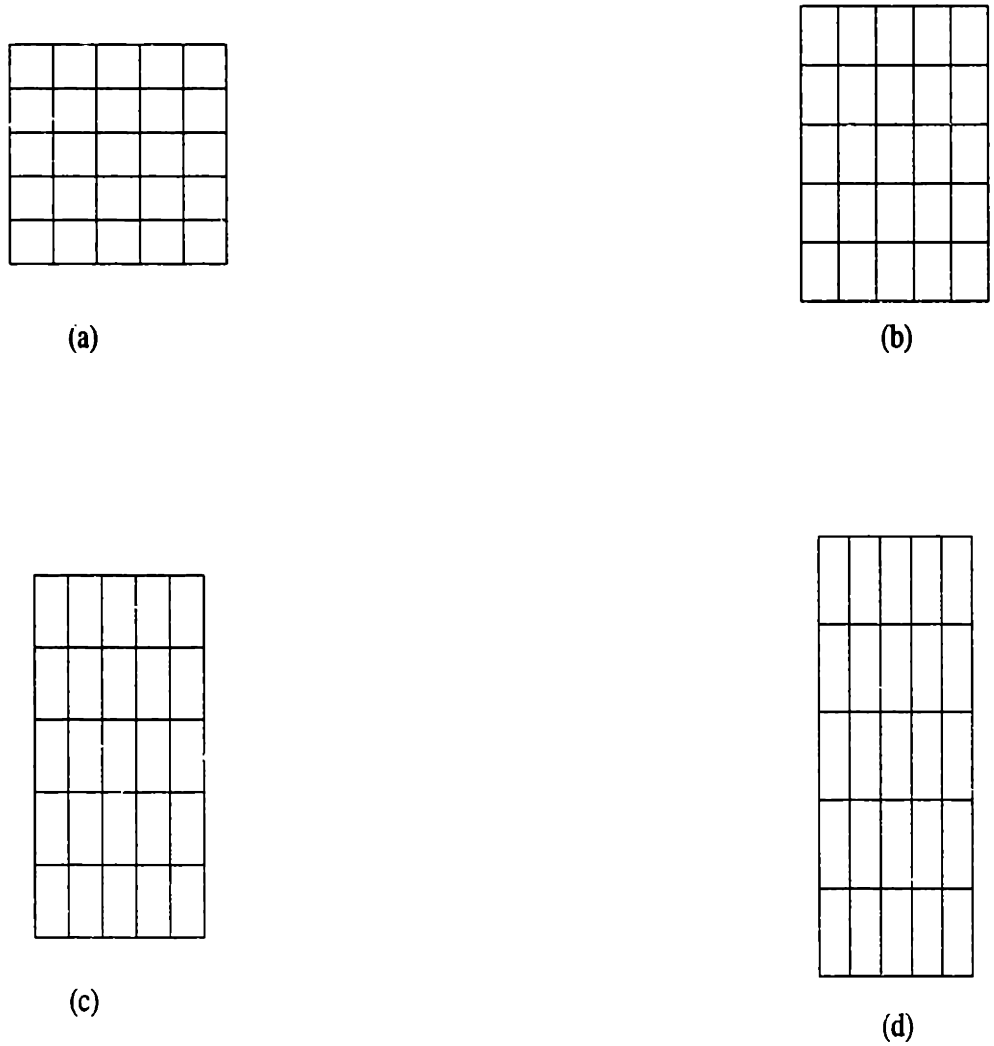

Figure 3.4: Uniaxial Tensile Deformation of V-BCC with 15% Vf: (a) E_z=0.0, (b) E_z=0.3, (c) E_z=0.5, (d) E_z=0.7

3.1.2 Stress vs. Strain Behavior

Through tension tests we can study the macroscopic stress-strain behavior of filled Chloroprene rubber. The homopolymer was included in comparing the stress vs. strain behavior in order to see how filler particles actually affect the mechanical behavior of the elastomer.

Figure 3.5 illustrates the axial stress versus axial strain for the homopolymer, 10% volume fraction, 15% volume fraction, and the 20% volume fraction. The larger the volume fraction the stiffer the macroscopic behavior of the unit voronoi cell. By looking at the graph we can also see that the stresses in the model almost double when comparing the homopolymer to the 20% filled elastomer at a strain of 0.7. We can also assume that as the strain continues to increase in the filled elastomers the difference in stresses between the different volume fractions increases since the curves tend to diverge from each other. The relationship between the stress/strain behavior is exponential.

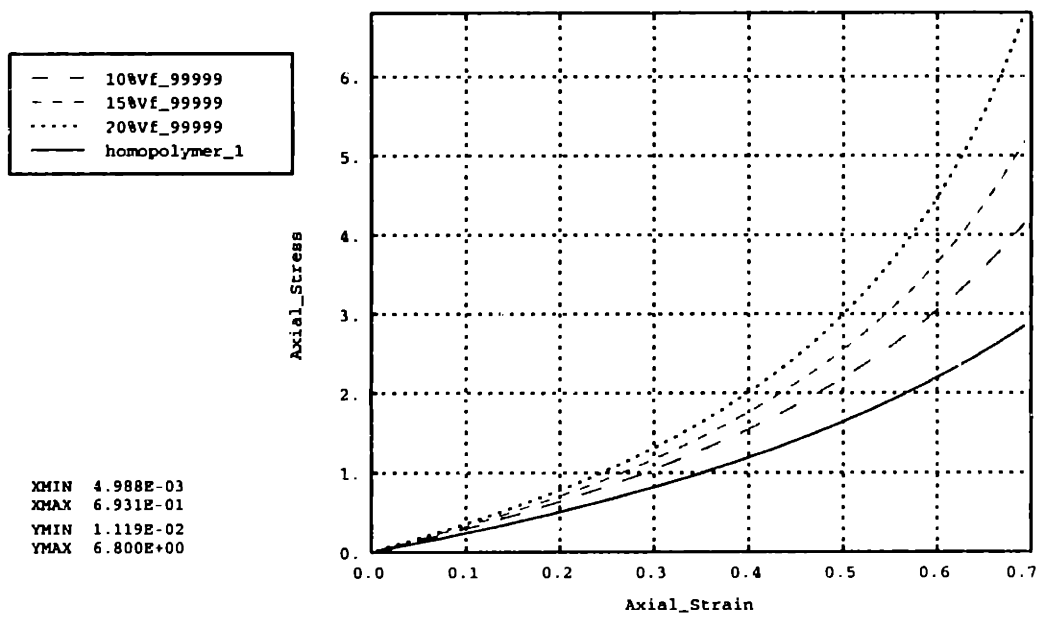

Figure 3.5: 100% Tension - V-BCC Model:Stress vs. Strain

3.1.3 Tangent Modulus versus Axial Strain

To compare the tangent modulus with the axial strain, the data was extracted from the Stress vs. Strain curves where the tangent modulus is simply the slope of the stress/strain curve. Figure 3.6 depicts the tangent modulus versus strain behavior for tensile uniaxial loading for the homopolymer, 10% volume fraction, 15% volume fraction, and 20% volume fraction models. The material stiffness increases as the volume fraction of the particle increases. However we can see that the slope increases on all the curves as the strain is increased; particularly for the 20% volume fraction where we can see that the curve is almost vertical and hence will eventually reach an infinite tangent modulus as the strain is increased. This simply means that the material can only be stretched to a finite length and if this length is surpassed then tearing processes come into play. Matrix materials with higher volume fractions of filler particle approach an infinite value for the tangent modulus more quickly than lower volume fractions. As we keep increasing the elastomer with more and more particles the stiffer the material will become and will loose it's compliance and behave mechanically more and more like a rigid material.

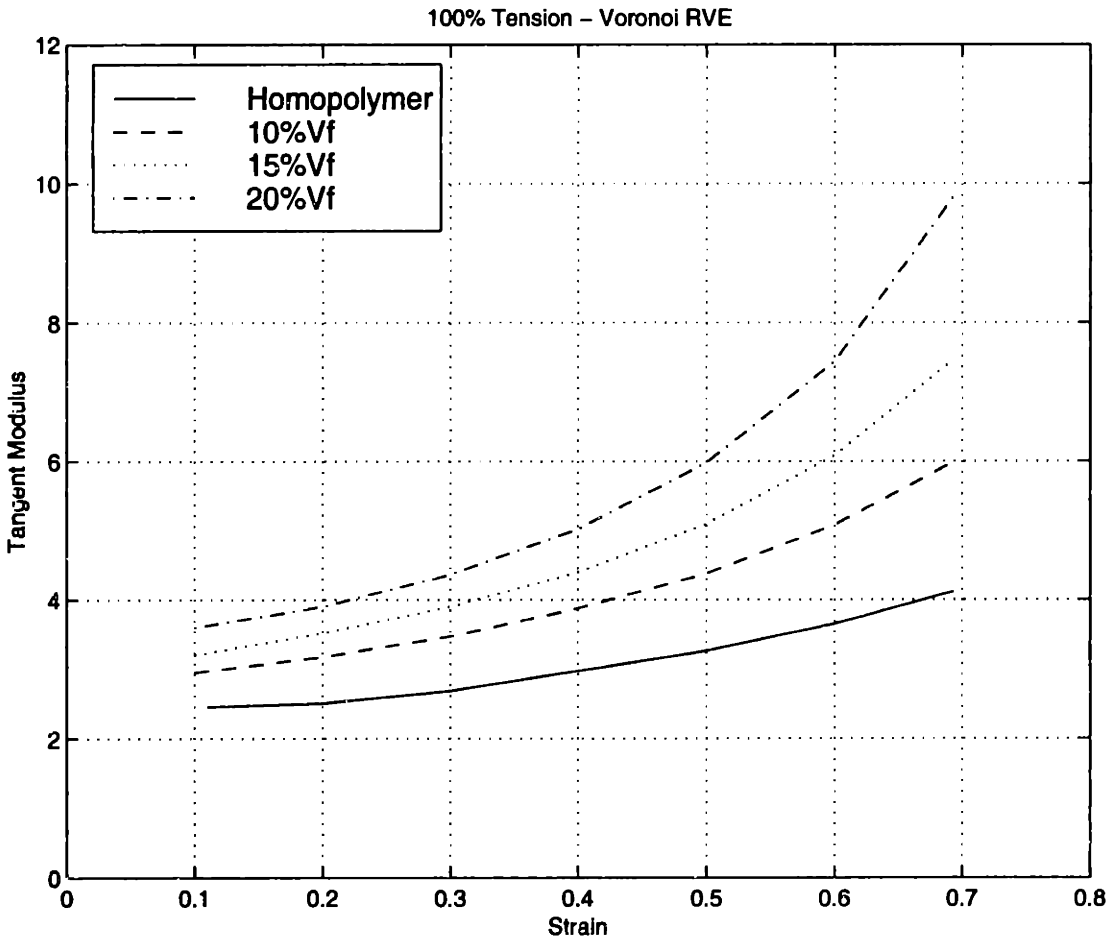

Figure 3.6: Tangent Modulus vs. Strain - Voronoi - BCC Model

3.1.4 Tangent Modulus versus Volume Fraction

Figure 3.7 illustrates the behavior between tangent modulus and volume fraction at various applied tensile strains. The undeformed model, $E_z = 0.0$, has a tangent modulus that increases linearly as the volume fraction of filler particles is increased. However, as the matrix material is subjected to larger tensile strains the tangent modulus increases at a faster rate in an exponential manner. Materials with lower volumes of filler particles will be able to reach higher strain values and thus stretch more.

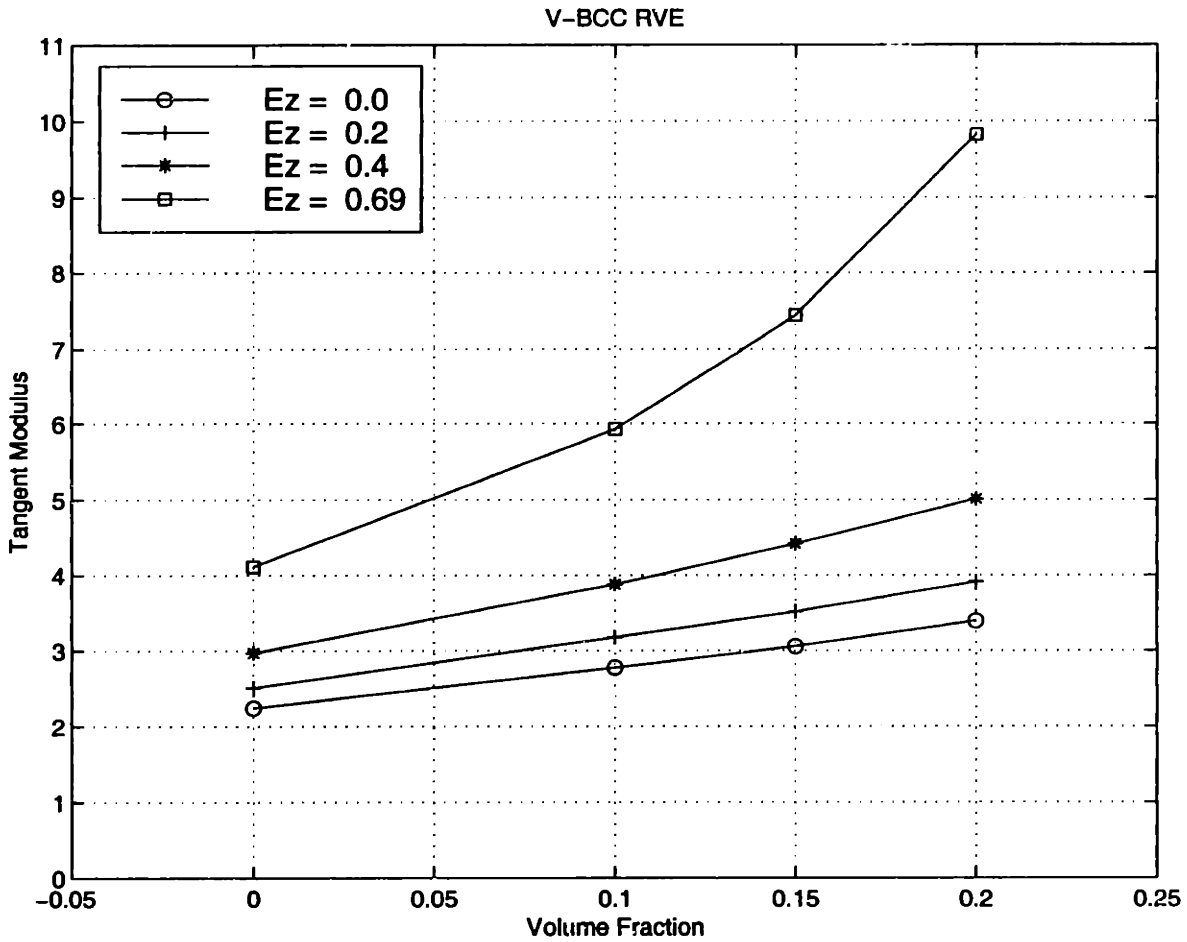

Figure 3.7: Tangent Modulus versus Volume Fraction for Tensile Loading

3.1.5 Axial Strain

Contour strain plots are shown for 10%, 15% and 20% volume fractions in Figures 3.8 through 3.10 respectively. Figure 3.8 illustrates the local axial strains of the matrix material as the mesh evolves from an applied macroscopic tensile axial strain of E_z=0.1 to E_z=0.7 in strain increments of 0.2. Since the matrix is perfectly adhered to the particle, as discussed previously in section 3.1.1, the local strains laterally adjacent to the material are between 0-20% of the applied macroscopic axial strain. Thus the imposed strain is accommodated for by the amplified stretching of the material above the particle which is approx-

imately 1.5 to 2 times greater than the applied strain. The amplified stretching is further discussed in the contour plots of the first stretch invariant in following section. Figures 3.9 and 3.10 depict similar localized strain behavior with even greater local strain values due to the increase volume fraction of filler particle.

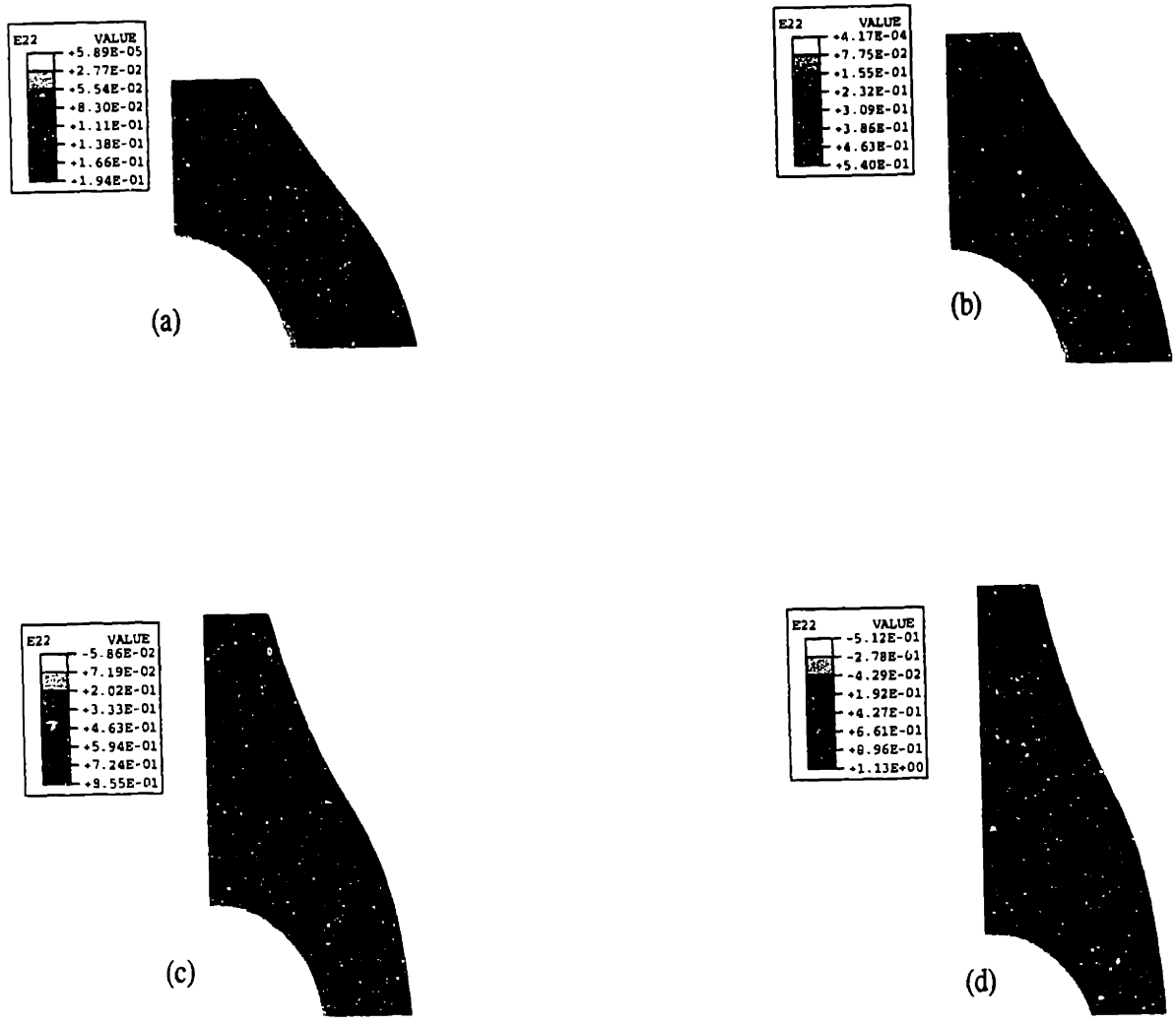

Figure 3.8: Tensile Axial Strain of V-BCC with 10% Vf: (a) E_z=0.1, (b) E_z=0.3, (c) E_z=0.5, (d) E_z=0.7

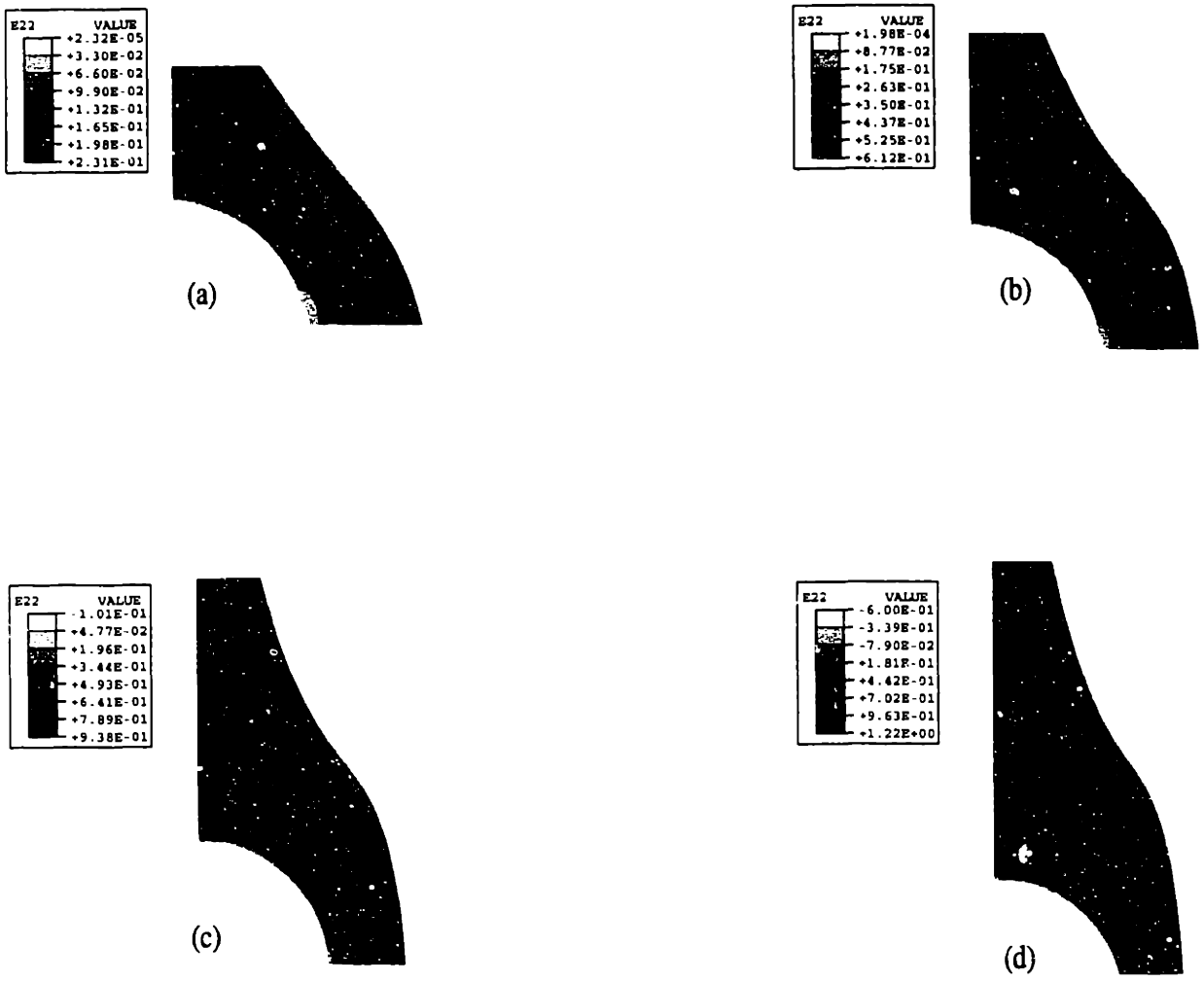

Figure 3.9: Tensile Axial Strain of V-BCC with 15% Vf: (a) E_z=0.1, (b) E_z=0.3, (c) E_z=0.5, (d) E_z=0.7

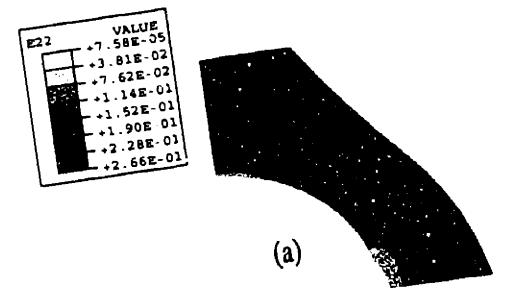

(a)

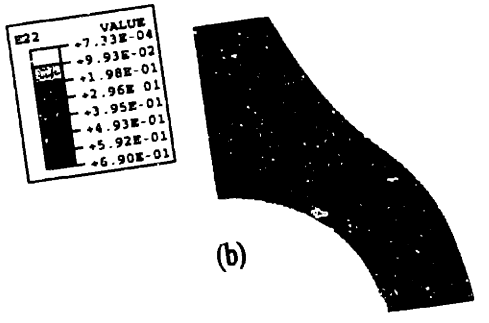

(b)

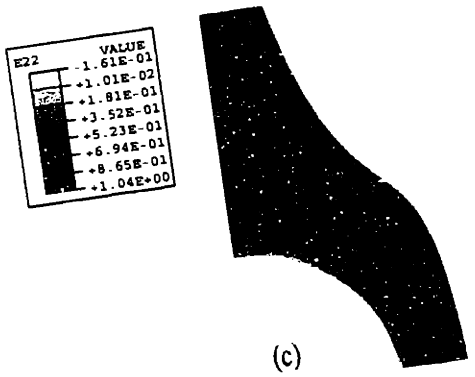

(c)

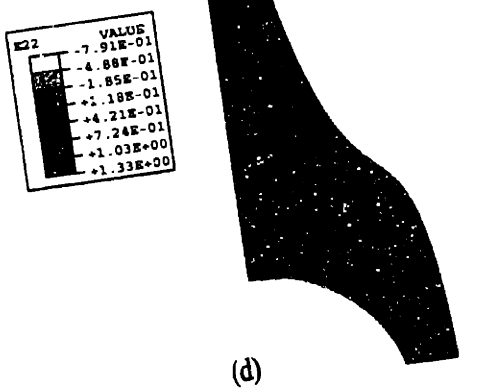

(d)

Figure 3.10: Tensile Axial Strain of V-BCC with 20% Vf: (a) E_z=0.1, (b) E_z=0.3, (c) E_z=0.5, (d) E_z=0.7

3.1.6 First Stretch Invariant

Contour plots of the first stretch invariant are shown for 10%, 15% and 20% volume fractions in Figures 3.11 through 3.13 respectively. The first stretch invariant is defined as $I_1=\lambda_1^2 + \lambda_2^2 + \lambda_3^2$, where λ_1, λ_2, and λ_3 are the principal stretches. An $I_1 = 3$ indicates no stretching. Figure 3.11 illustrates the local first stretch invariant of the matrix material as the mesh evolves from an applied macroscopic tensile axial strain of E_z=0.1 to E_z=0.7 in strain increments of 0.2. The applied I_1 for applied axial strains of 0.1, 0.3, 0.5 and 0.7 are 3.03, 3.30, 3.93, and 5.04 respectively. The contours again show regions of negligible stretching diagonally between particles ($I_1 \approx 3$) and highly amplified stretching above the particle where the loading is applied.

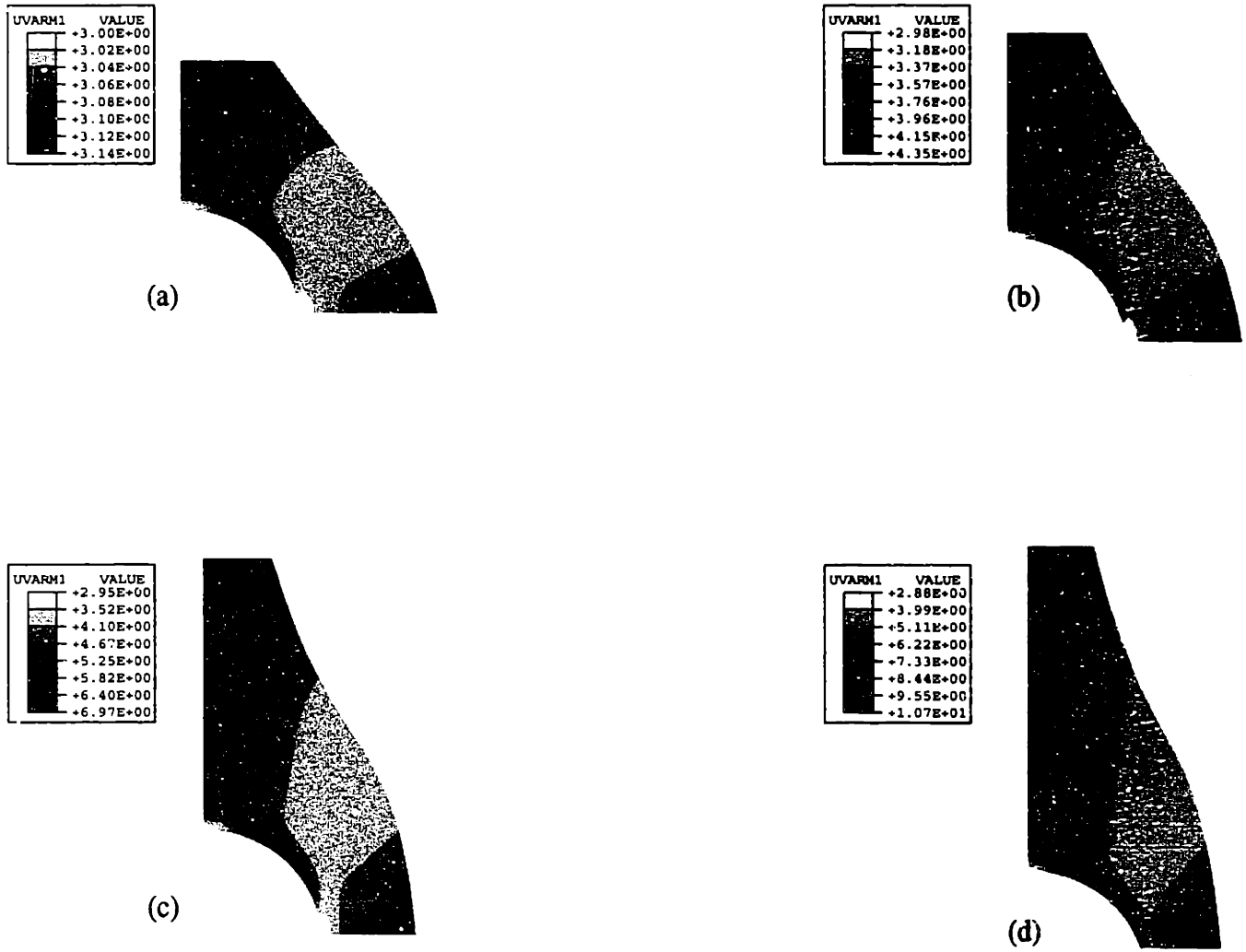

Figure 3.11: First Strain Invariant of V-BCC in Tension 10% Vf: (a) E_z=0.1, (b) E_z=0.3, (c) E_z=0.5, (d) E_z=0.7

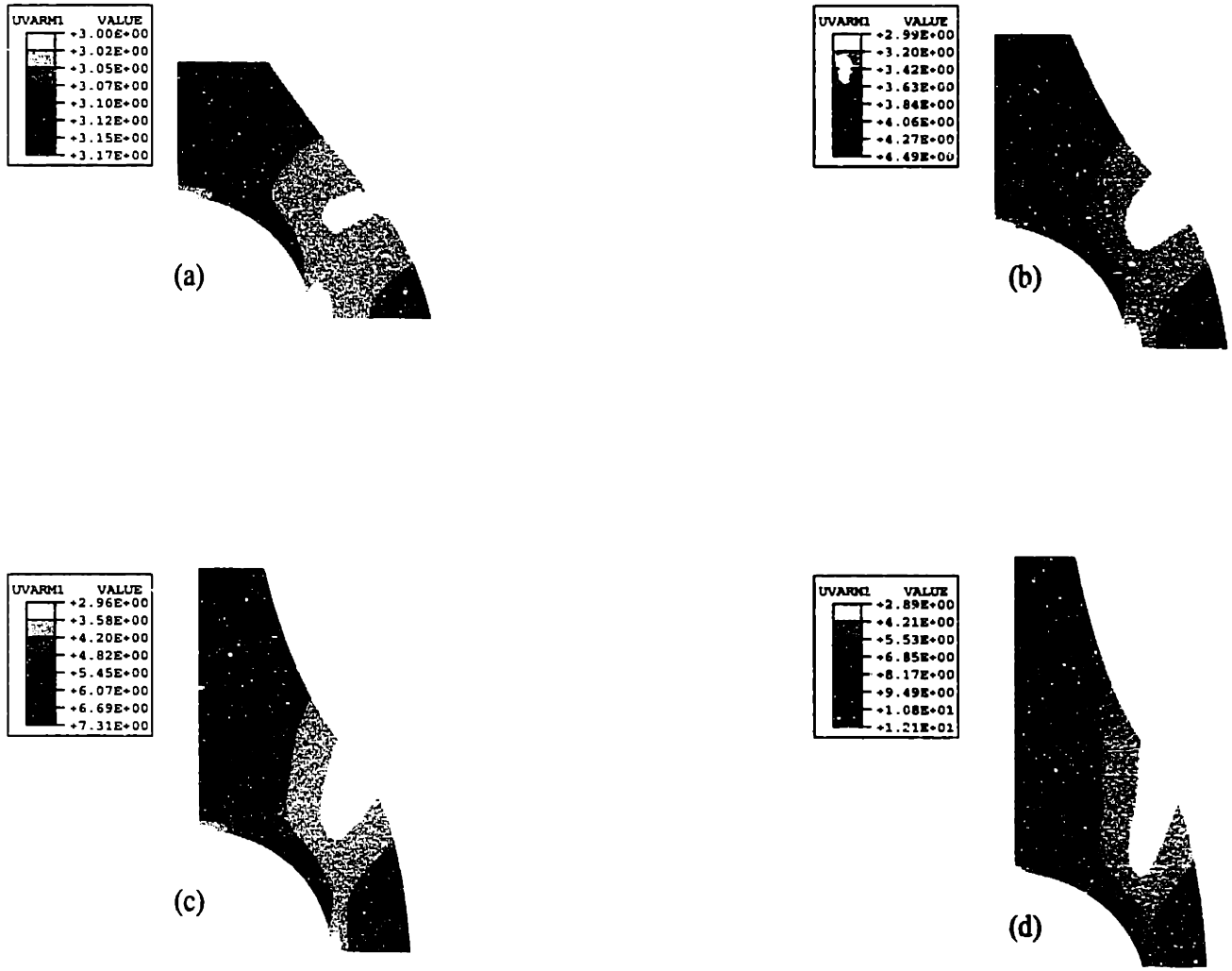

Figure 3.12: First Strain Invariant of V-BCC in Tension 15% Vf: (a) E_z=0.1, (b) E_z=0.3, (c) E_z=0.5, (d) E_z=0.7

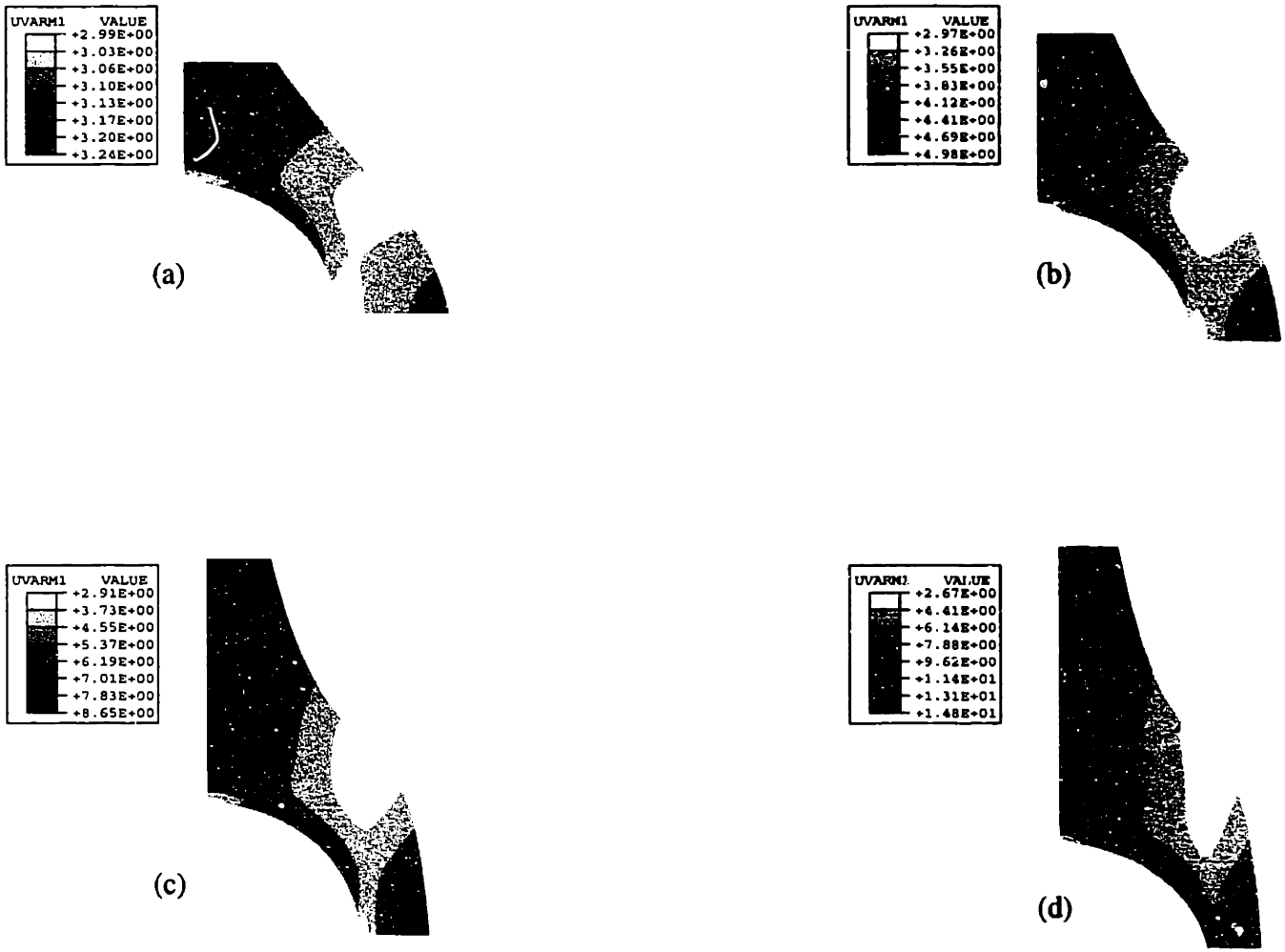

Figure 3.13: First Strain Invariant of V-BCC in Tension 20% Vf: (a) E_z=0.1, (b) E_z=0.3, (c) E_z=0.5, (d) E_z=0.7

3.1.7 Axial Stress

Contour stress plots are shown for 10%, 15% and 20% volume fractions in Figures 3.14 through 3.16 respectively. Figure 3.14 illustrates the local axial stresses of the matrix material as the mesh evolves from an applied macroscopic tensile axial strain of E_z=0.1 to E_z=0.7 in strain increments of 0.2. The local stresses are largest directly above the filler particle since loading is tensile in the axial direction and stretching is amplified there as discussed earlier. These stresses are approximately 3 times greater than the macroscopic cell stress as seen in Section 3.1.2. The local stresses are smallest to the right of the particle and are about 1/3 the value of the macroscopic stress. It can also be seen that the local stress is approximately equal to the macroscopic stress at the vertical center of the contour plots. Figures 3.9 and 3.10 depict similar localized stress behavior with even greater local stress values due to the increased volume fraction of filler particles.

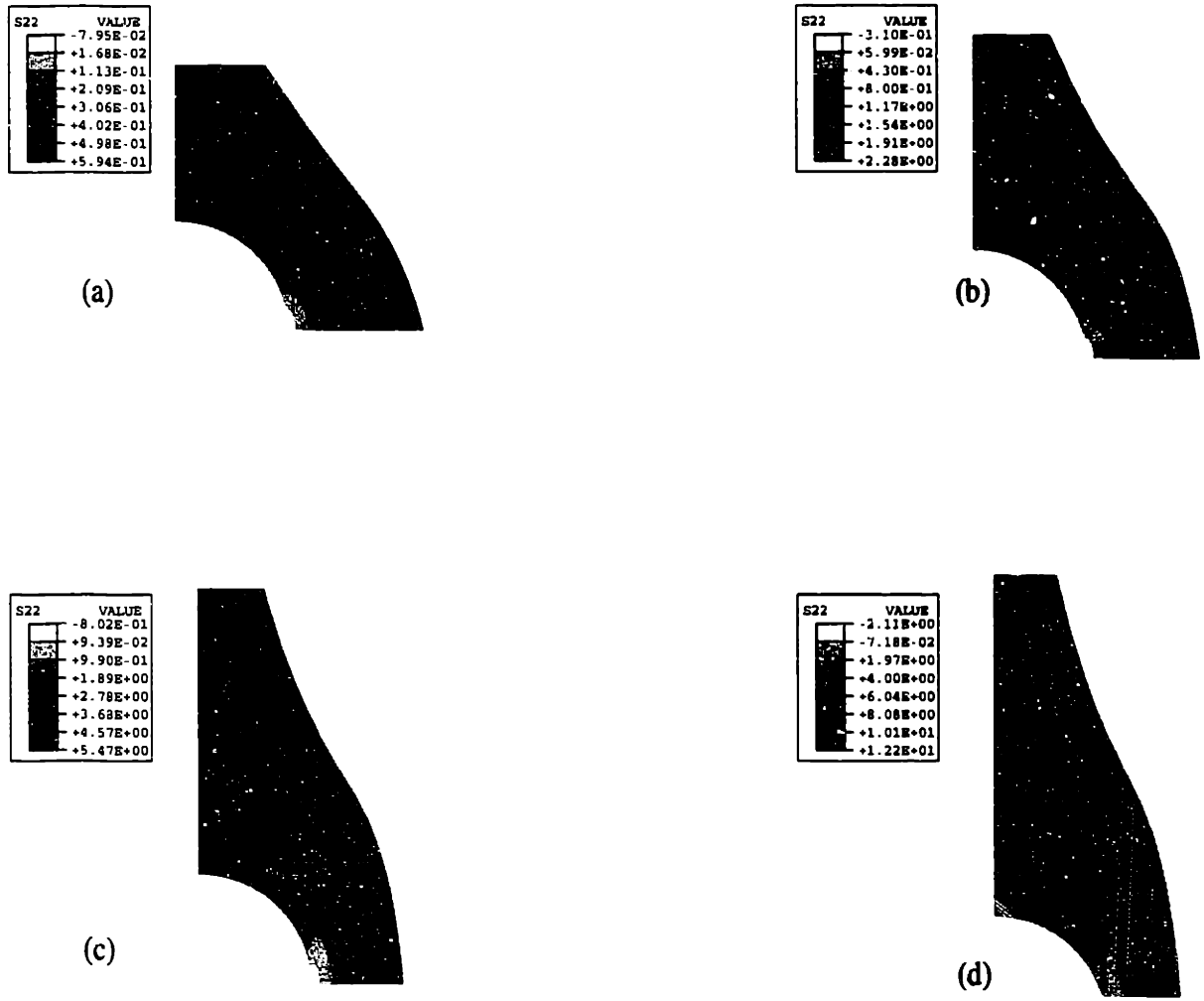

Figure 3.14: Tensile Axial Stress of V-BCC for 10% Vf: (a) E_z=0.1, (b) E_z=0.3, (c) E_z=0.5, (d) E_z=0.7

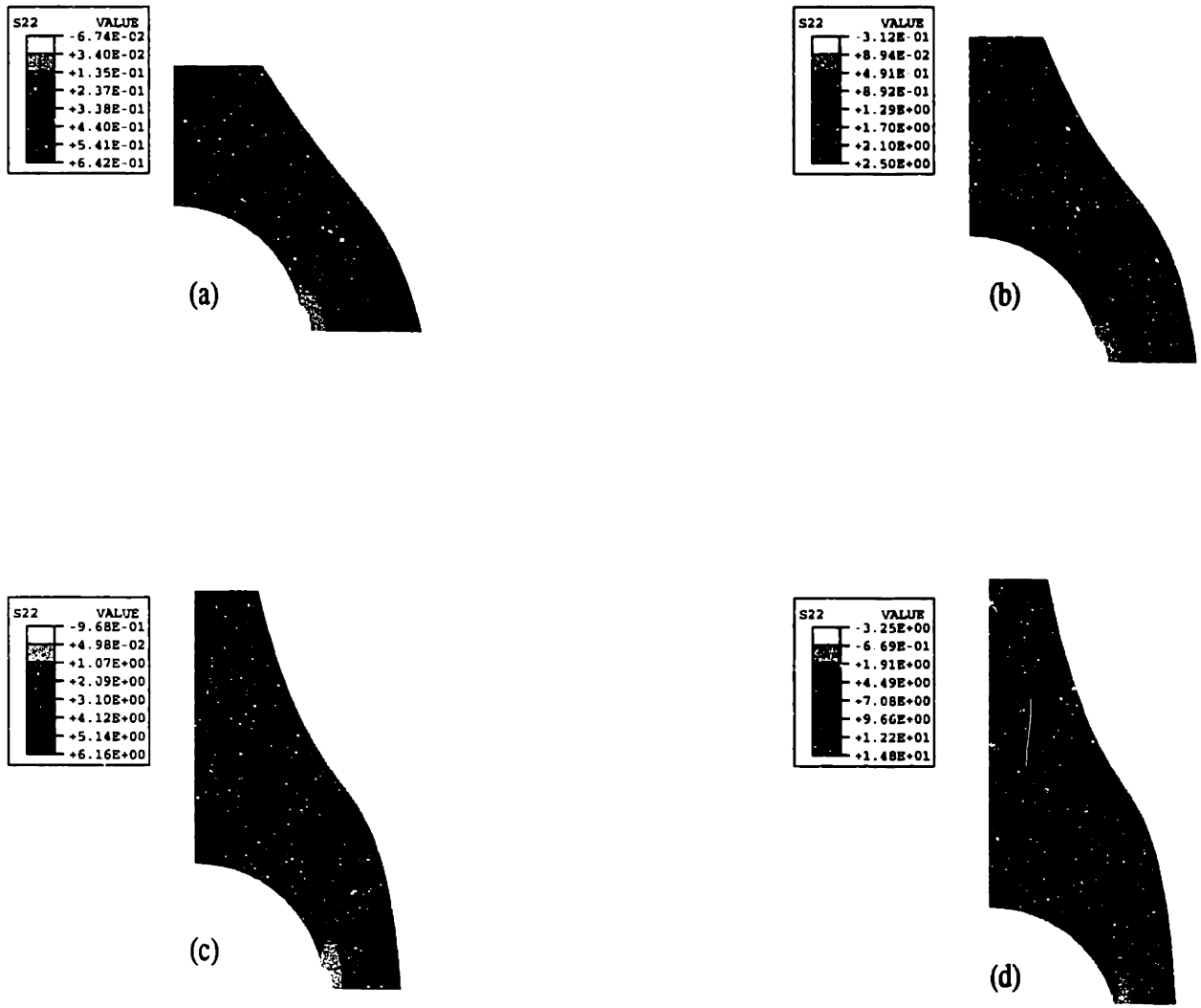

Figure 3.15: Tensile Axial Stress of V-BCC for 15% Vf: (a) E_z=0.1, (b) E_z=0.3, (c) E_z=0.5, (d) E_z=0.7

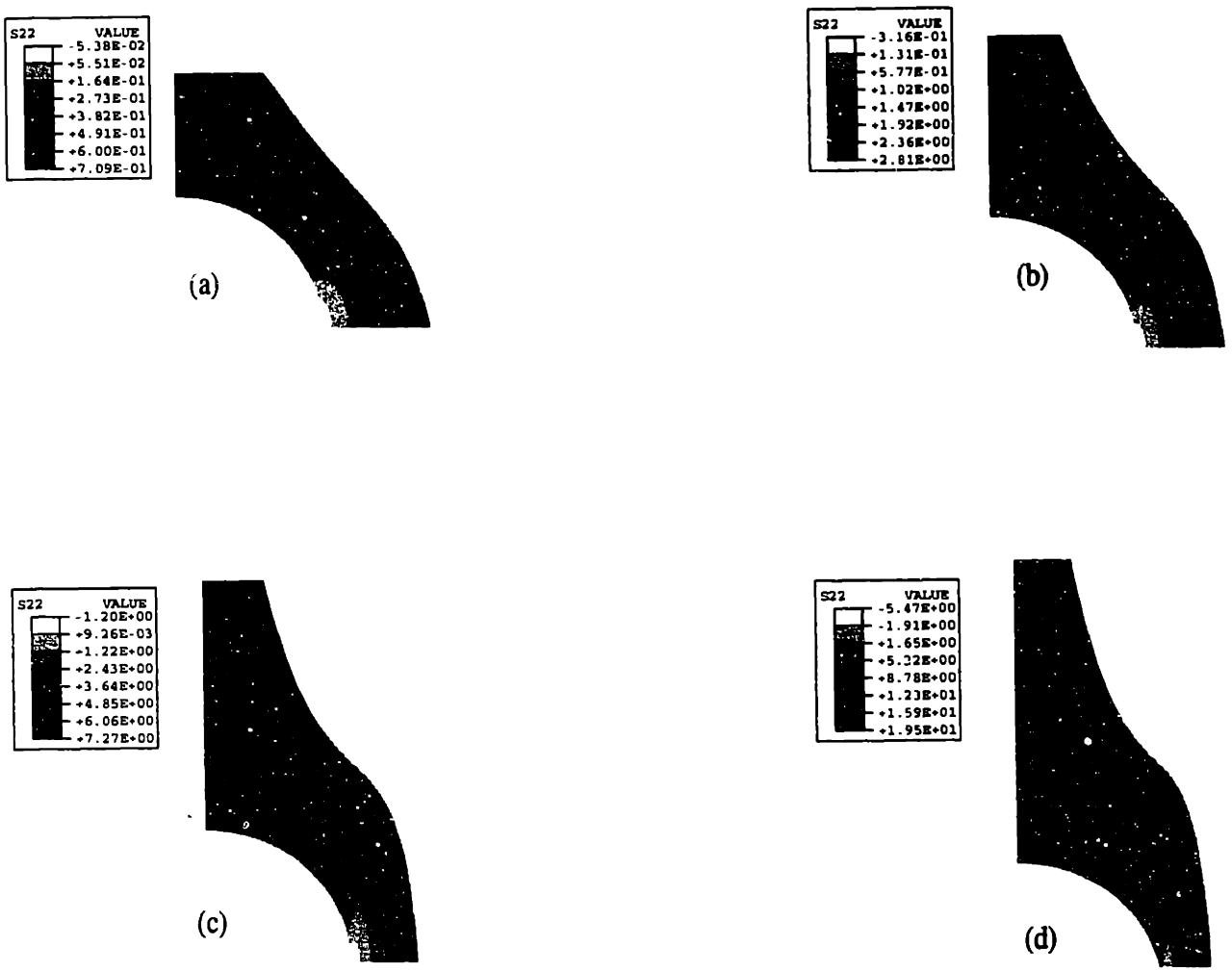

Figure 3.16: Tensile Axial Stress of V-BCC for 20% Vf: (a) E_z=0.1, (b) E_z=0.3, (c) E_z=0.5, (d) E_z=0.7

3.2 Compression

3.2.1 Deformation

The filled chloroprene rubber V-BCC RVE model was deformed to a final macroscopic axial strain of -0.36 at a constant strain rate of -0.1 s^{-1}. The same logarithmic strain measure, $\varepsilon = \ln\left(\frac{h}{h_o}\right)$, was used as was for tension.The final length of the filled elastomer is therefore 7/10 of its original height (30% nominal compression). Figures 3.16 through 3.19 illustrate the deformation of the elastomer where deformed meshes are depicted at strains of 0.0, -0.20, -0.30 and -0.36 for volume fractions of 10%, 15%, 20%, and the homopolymer respectively.

In Figure 3.16, the evolution in the deformation of the mesh with macroscopic axial strain illustrates how the matrix is deforming locally in order to accommodate the imposed strain. Since the matrix is perfectly adhered to the particle, there is little axial strain observed in the material laterally adjacent to the particle and the imposed strain is accommodated by amplified axial compression and radial stretching of the material above the particle. This effect is discussed further in sections 3.2.5 and 3.2.7 when contours of matrix strain and stress are examined.

Figures 3.17 and 3.18 depict similar responses as discussed for Figure 3.16 where the matrix deformation is even further amplified because of higher volume fractions with filler particles. The homopolymer, Figure 3.19, has uniform matrix deformation such that there is uniform stretching of the matrix in the radial direction and thus has a constant strain throughout the matrix.

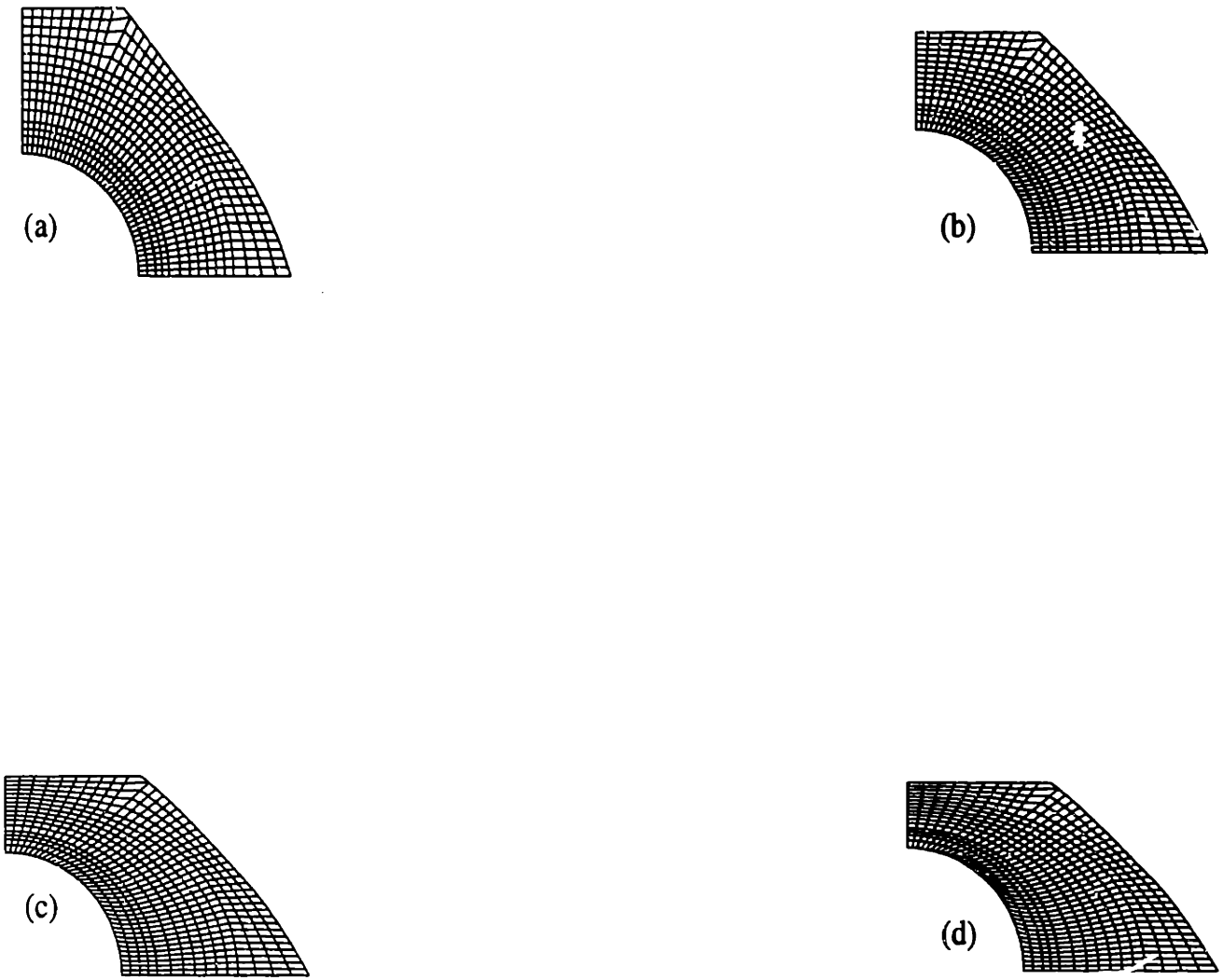

Figure 3.17: Uniaxial Compressive Deformation of V-BCC with 10% Vf: (a) E_z=0.0, (b) E_z=0.2, (c) E_z=0.3, (d) E_z=0.36

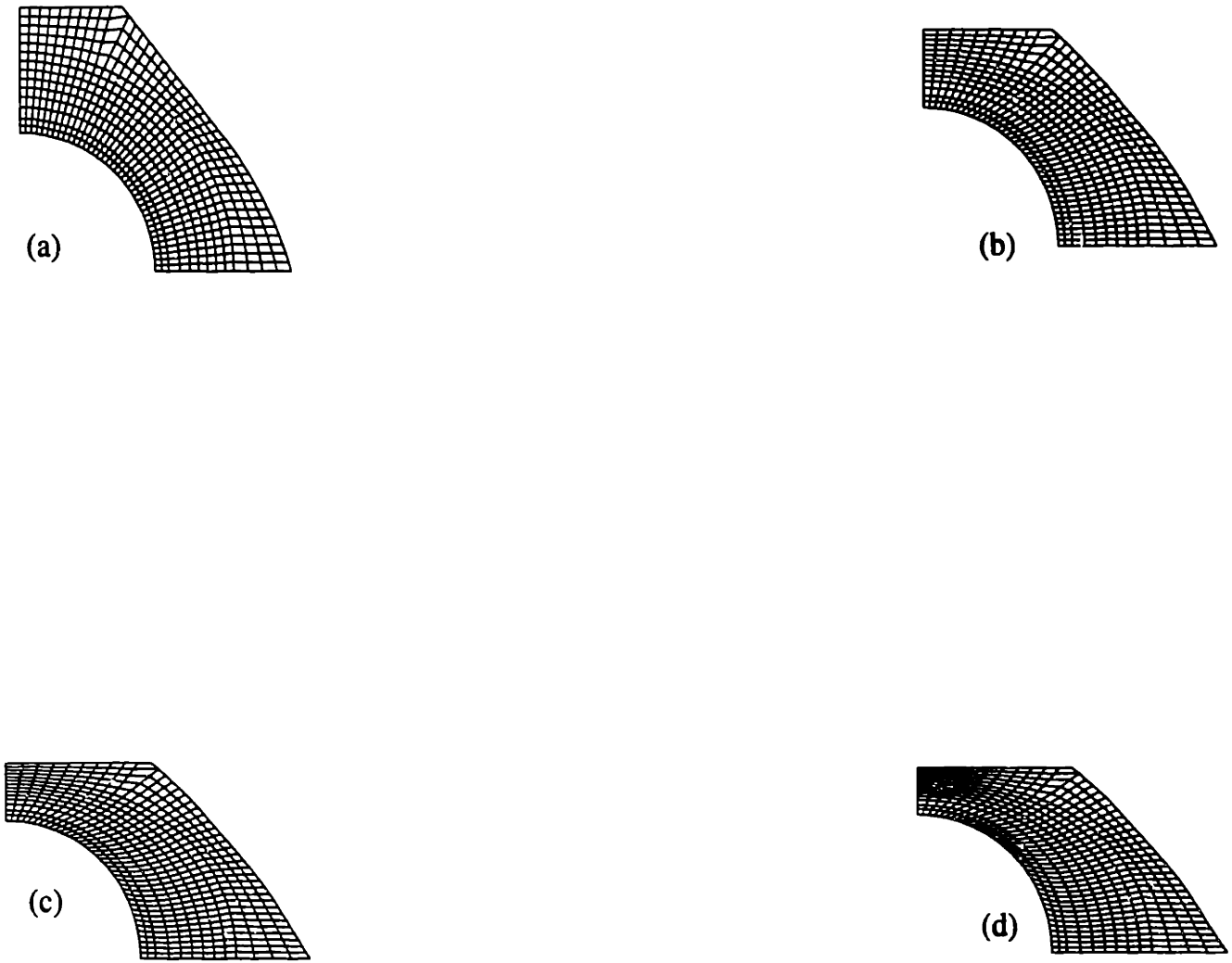

Figure 3.18: Uniaxial Compressive Deformation of V-BCC with 15% Vf: (a) E_z=0.0, (b) E_z=0.2, (c) E_z=0.3, (d) E_z=0.36

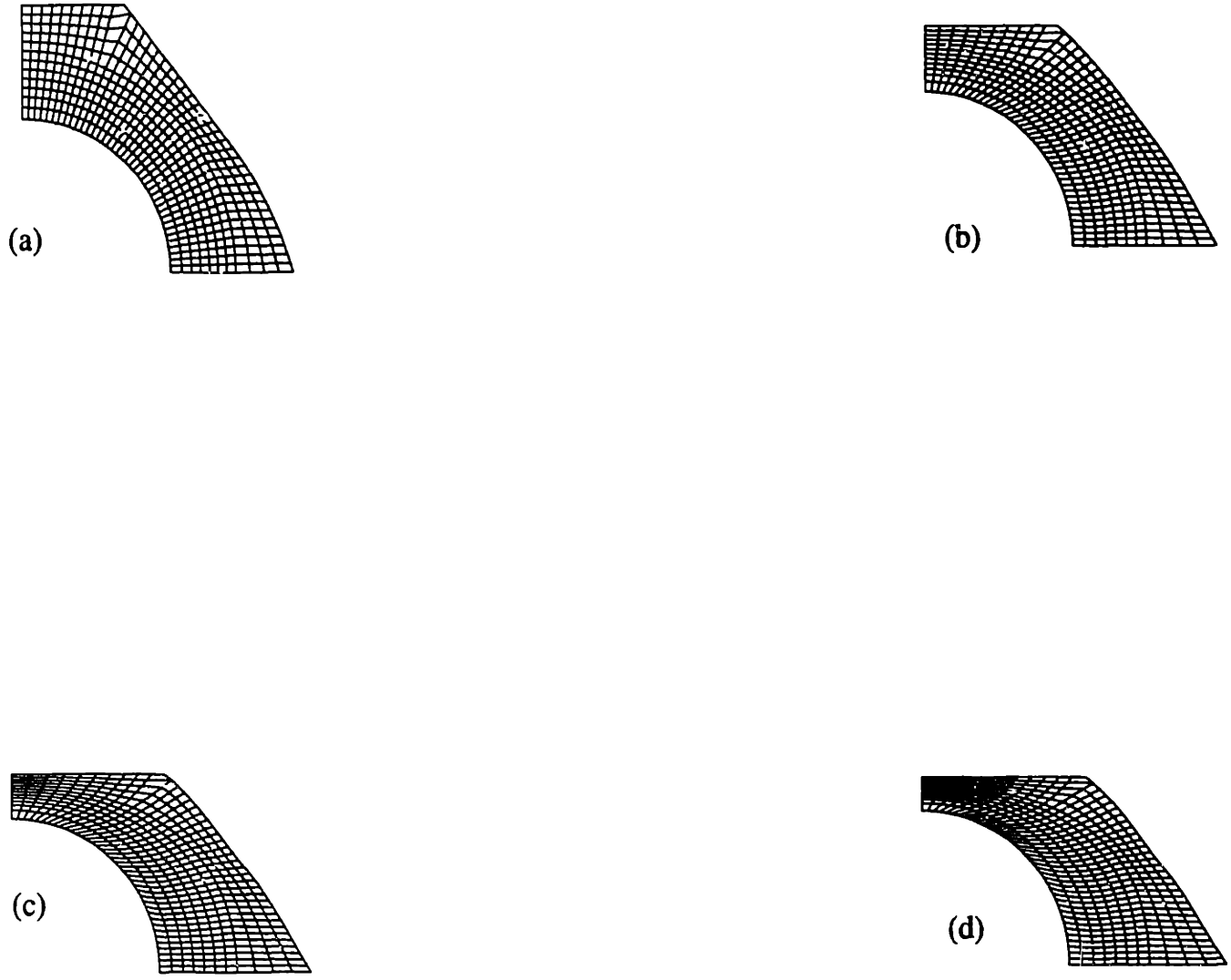

Figure 3.19: Uniaxial Compressive Deformation of V-BCC with 20% Vf: (a) E_z=0.0, (b) E_z=0.2, (c) E_z=0.3, (d) E_z=0.36

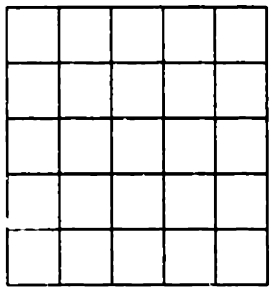

(a)

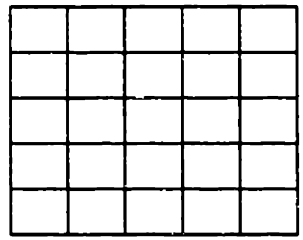

(b)

(c)

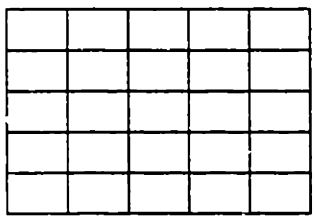

(d)

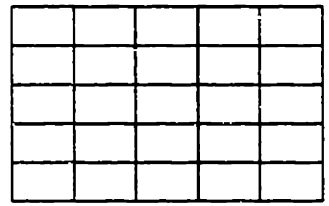

Figure 3.20: Uniaxial Compressive Deformation of Homopolymer (a) E_z=0.0. (b) E_z=0.2, (c) E_z=0.3, (d) E_z=0.36

3.2.2 Stress-Strain Behavior

In Figure 3.21 the macroscopic axial stress versus axial strain behavior for the homopolymer, 10% volume fraction, 15% volume fraction, and the 20% volume fraction of the Voronoi model unit cell are shown when subjected to 30% uniaxial compression. The graph is plotted against a positive xy axis; however, the actual stress and strain values for compression are negative in magnitude. We can see that the larger the volume fraction the larger the macroscopic stresses in unit voronoi cell just as seen in Figure 3.5 for tension. By looking at the graph we can also see that the stresses in the model almost double when comparing the homopolymer to the 20% filled elastomer at a strain of 0.35. We can also assume that as the strain continues to increase in the filled elastomers the difference in stresses between the different volume fractions increases since the curves tend to diverge from each other. In the compression stress-strain behavior the relationship looks linear while in tension, Figure 3.5, they appear to be exponential.

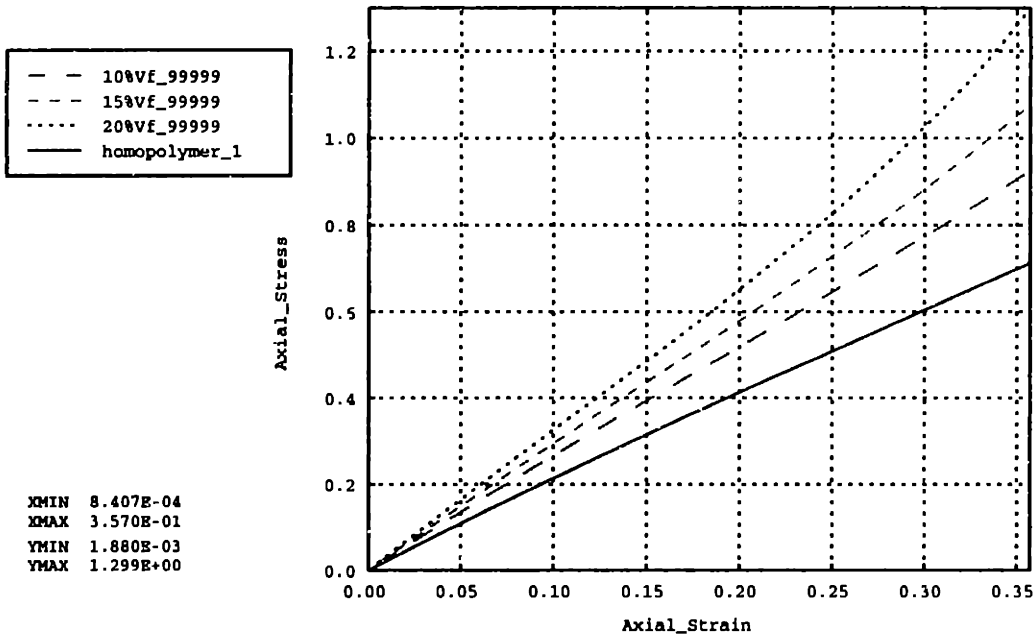

Figure 3.21: 30% Compression - Voronoi- BCC Model

3.2.3 Tangent Modulus versus Axial Strain

The relationship between the tangent modulus and strain for the unit cell when subjected to 30% compression can be seen in Figure 3.22 which illustrates both the compression and tension loading. Studying compression (the negative strain values) the tangent modulus of the homopolymer tends to become smaller as we approach greater strain magnitudes. According to the graph, the homopolymer will reach a steady state value for the tangent modulus as the matrix material is compressed to greater strains since the slope of the curve slowly decreases. This will be discussed further in section 3.2.4.

When a filler particle is added to the matrix material the tangent modulus initially decreases as we impose negative uniaxial strains and then begins to increase as larger strain magnitudes are imposed. This behavior can be depicted specifically in the 20% volume fraction curve. The material stiffness increases as Vf is increased. Since we do not

show a strain greater than E_z = -0.35 we assume that the curve will mirror the tension behavior and reach an infinite stiffness as compressed to greater strains. It should also be noted that the material is subjected to uniaxial compression and therefore can only be compressed to the height (radius) of the filler particle since the particle is rigid.

Figure 3.22: Tangent Modulus versus Strain

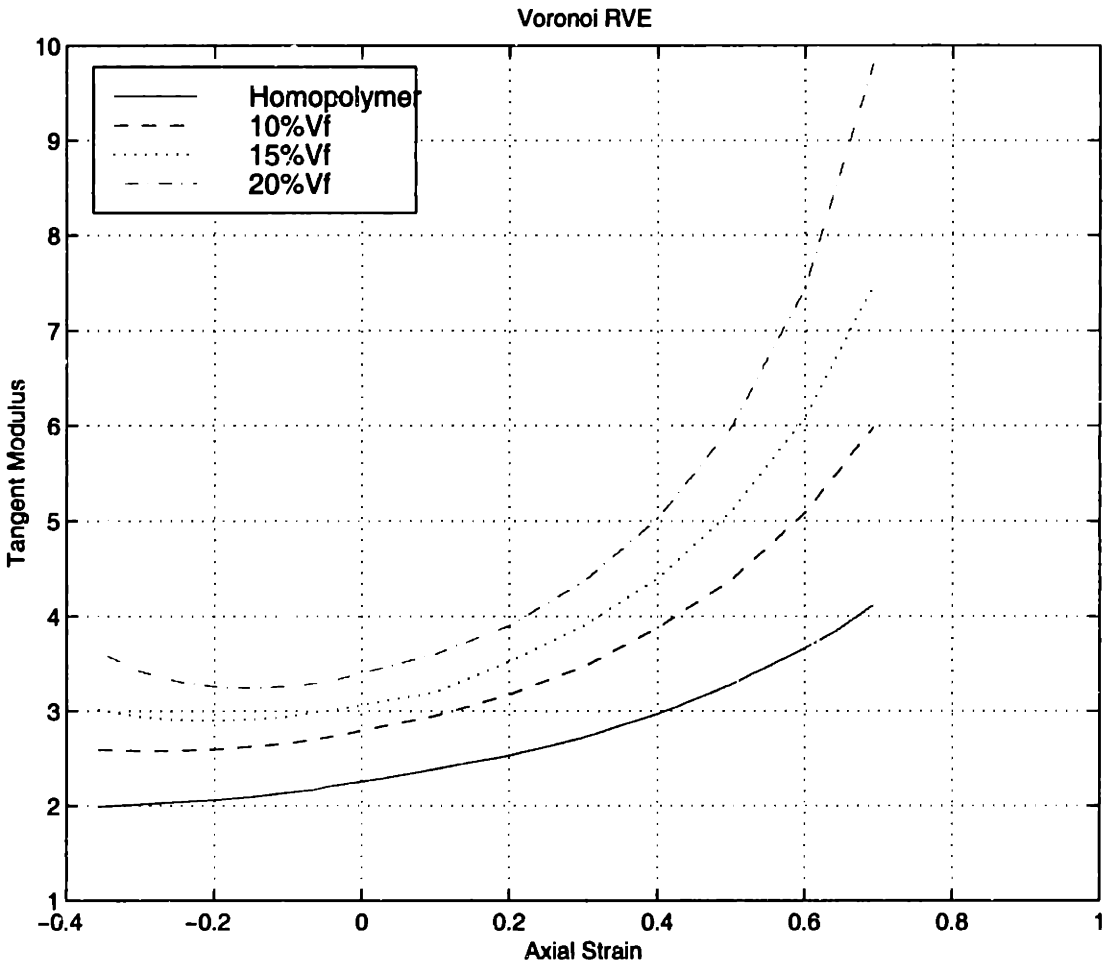

3.2.4 Tangent Modulus versus Volume Fraction

Figure 3.7 illustrates the behavior between tangent modulus and volume fraction ar various applied compressive strains. The undeformed model, $E_z = 0.0$, has a tangent modulus that increases linearly as the volume fraction of filler particles is increased. Notice how the tangent modulus is the same, approximately 3.25 MPa, for the strain curves $E_z = -.02$ and $E_z = -0.1$ for 20% volume fraction. This behavior is due to the parabolic behavior of the tangent modulus versus strain curves as seen previously in Figure 3.22 for the 20% volume fraction curve. This parabolic behavior can also be illustrated by the crossing of the compressive strain curves in Figure 3.23.

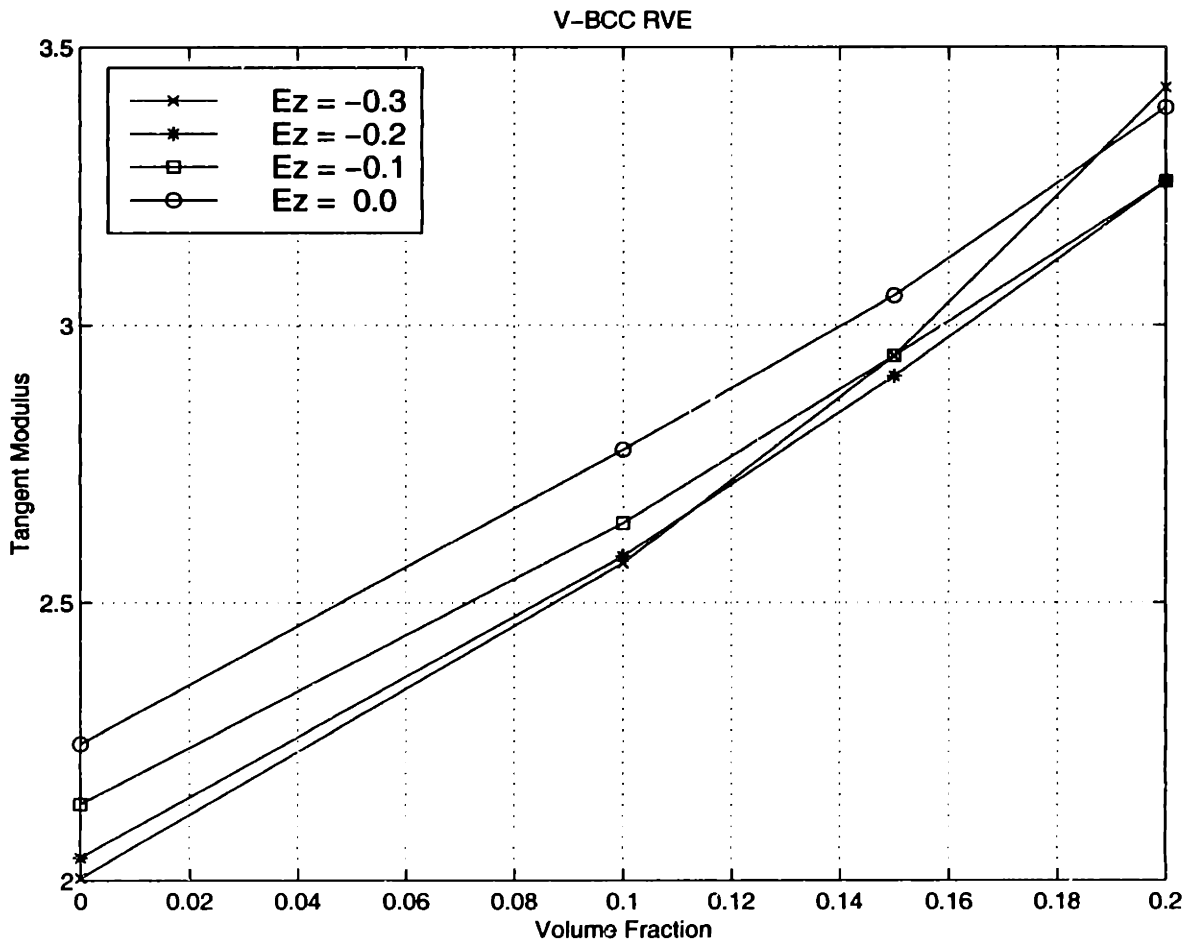

Figure 3.23: Tangent Modulus vs. Volume Fraction for Uniaxial Compressive Loading

3.2.5 Axial Strain

Contour strain plots are shown for 10%, 15% and 20% volume fractions in Figures 3.24 through 3.26 respectively. Figure 3.24 illustrates the local axial strains of the matrix material as the mesh evolves from an applied macroscopic compressive axial strain of E_z=-0.1 to E_z= -0.36. Since the matrix is perfectly adhered to the particle, as discussed previously in section 3.1.1, the local strains laterally adjacent to the material are between 0-20% of the applied macroscopic axial strain. Thus the imposed strain is accommodated for by the amplified stretching of the material above the particle which is approximately 1.5 to 2 times greater in magnitude than the applied strain. The amplified stretching is further discussed in the contour plots of the first stretch invariant in following section. Figures 3.25 and 3.26 depict similar localized strain behavior with even greater local strain values due to the increase volume fraction of filler particle. The local axial strain is also closest in value to the macroscopic axial strain near the center horizontal region of all the strain contour plots. The values of strain are noted by the magnitude; the negative value simply indicates the matrix is in compression.

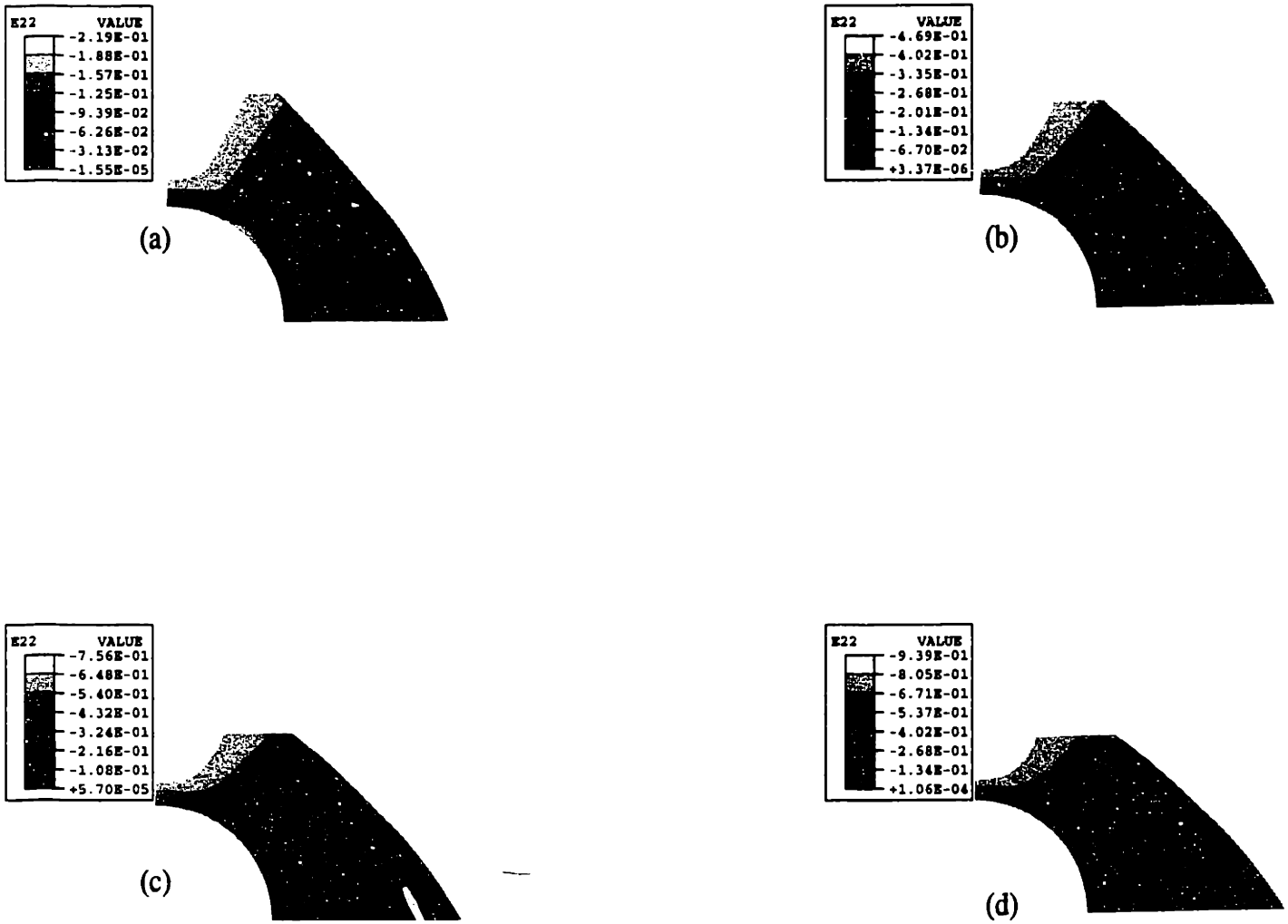

Figure 3.24: Compressive Axial Strain of V-BCC with 10% Vf: (a) Ez=0.1, (b) Ez=0.2, (c) Ez=0.3, (d) Ez=0.36

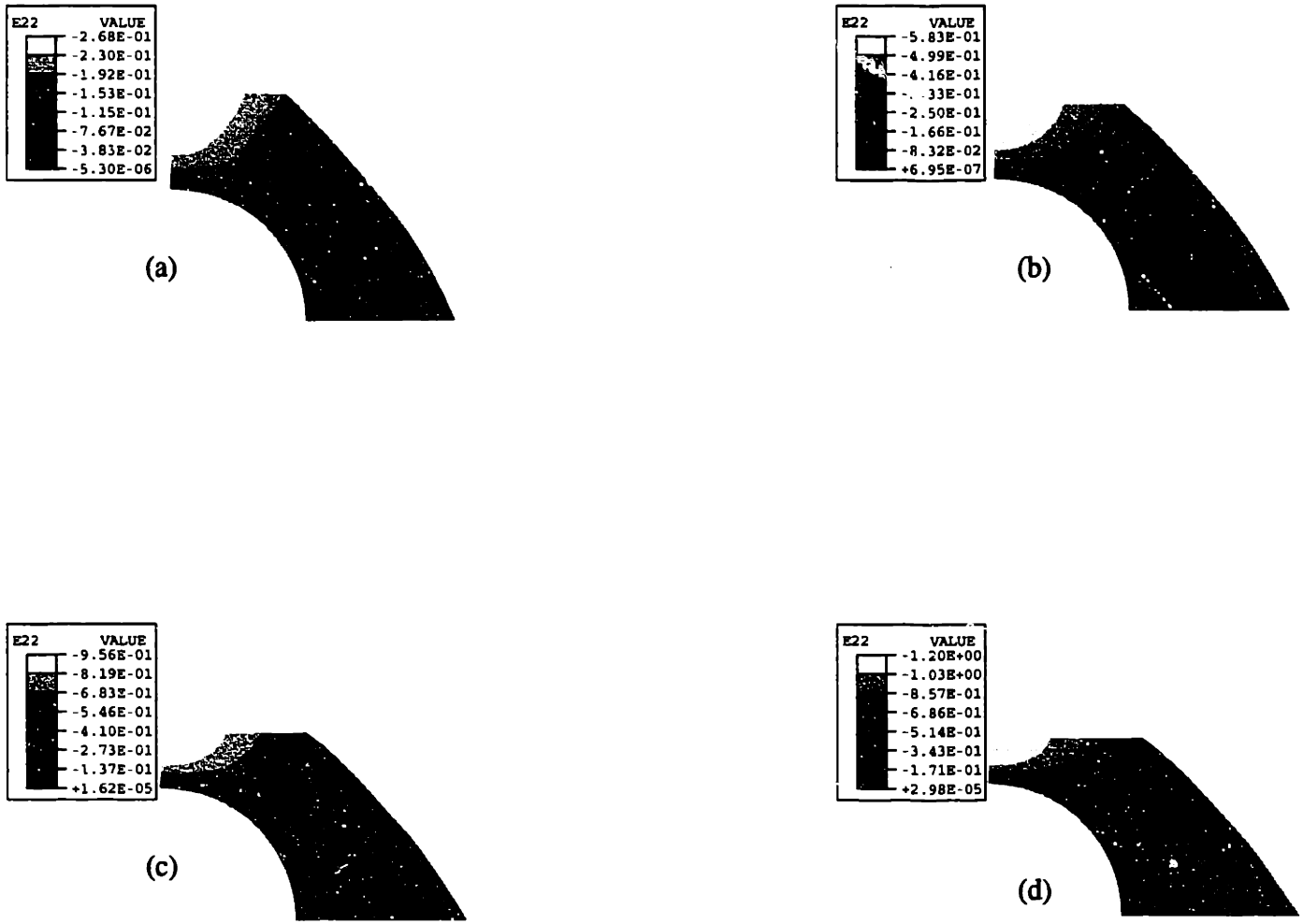

Figure 3.25: Compressive Axial Strain of V-BCC with 15% Vf: (a) Ez=0.1, (b) Ez=0.2, (c) Ez=0.3, (d) Ez=0.36

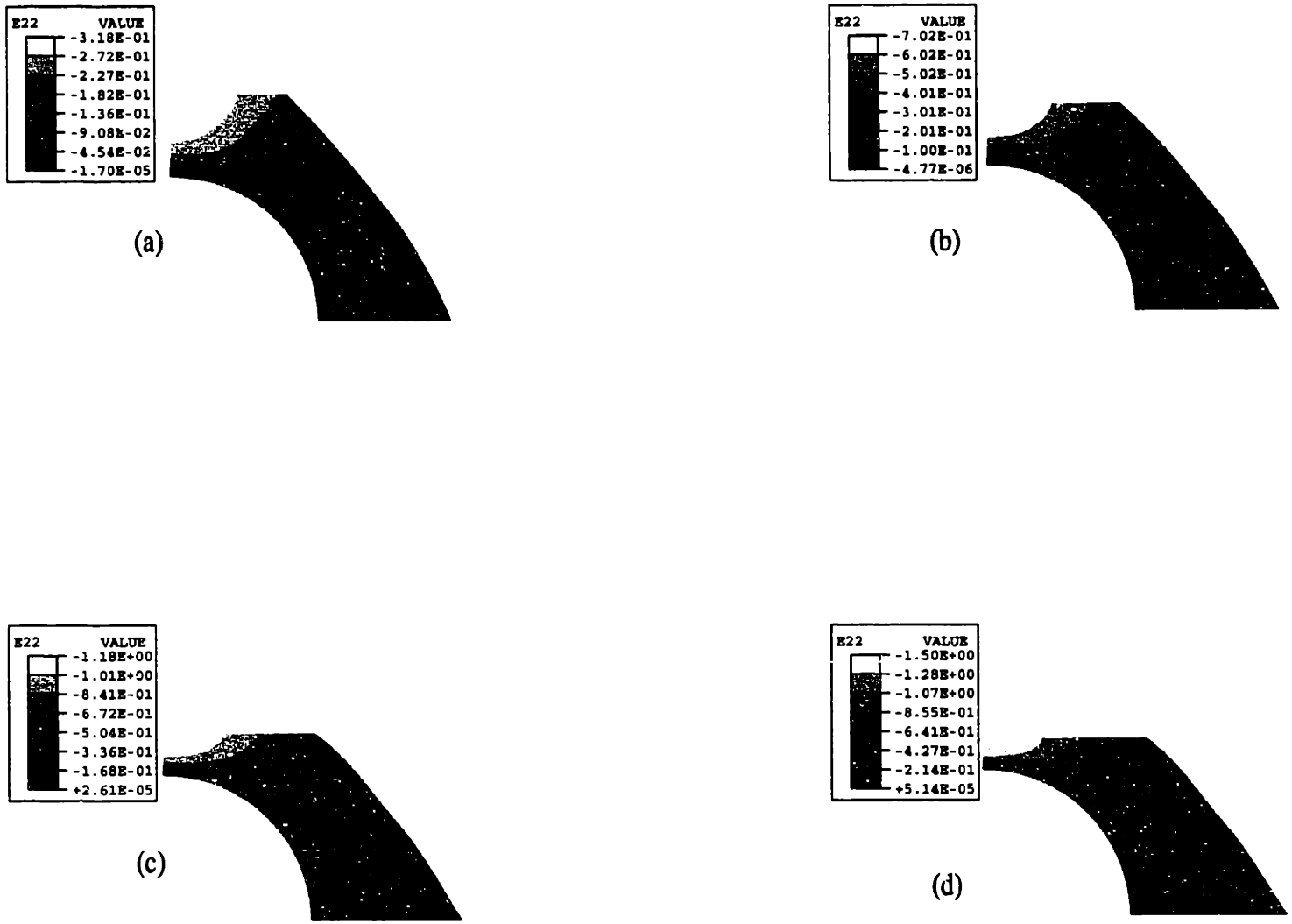

Figure 3.26: Compressive Axial Strain of V-BCC with 20% Vf: (a) Ez=0.1, (b) Ez=0.2, (c) Ez=0.3, (d) Ez=0.36

3.2.6 First Stretch Invariant

Contour plots of the first stretch invariant are shown for 10%, 15% and 20% volume fractions in Figures 3.27 through 3.29 respectively. The first stretch invariant is defined as $I_1=\lambda_1^2 + \lambda_2^2 + \lambda_3^2$, where λ_1, λ_2, and λ_3 are the principal stretches. As mentioned previously, $I_1=3$ indicates no stretching. Figure 3.27 illustrates the local first stretch invariant of the matrix material for applied macroscopic compressive axial strains of $E_z=-0.1$, $E_z=-0.2$, $E_z=-0.3$, and $E_z=-0.36$. The applied I_1 for those strains are 3.03, 3.11, 3.25, and 3.35 respectively. The contours again show regions of negligible stretching diagonally between particles and highly amplified stretching above the particle. There is less stretching in the compression contours than the tension contours when comparing the first stretch invariants. This is because the V-BCC model has smaller applied axial strains for compression and the material has more available space to expand in tension.

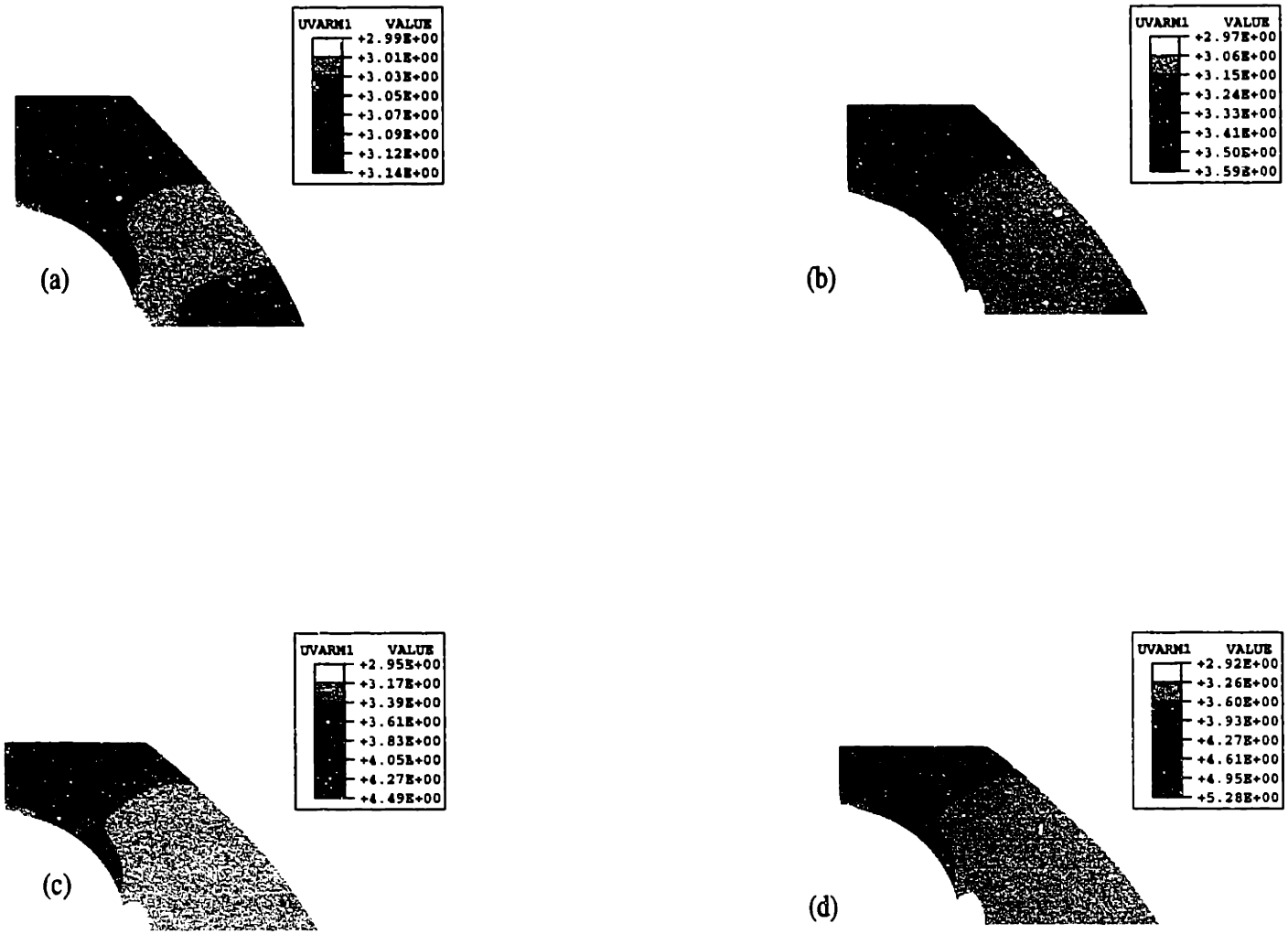

Figure 3.27: First Strain Invariant of V-BCC in Compression 10% Vf: (a) E_z=0.1, (b) E_z=0.2, (c) E_z=0.3, (d) E_z=0.36

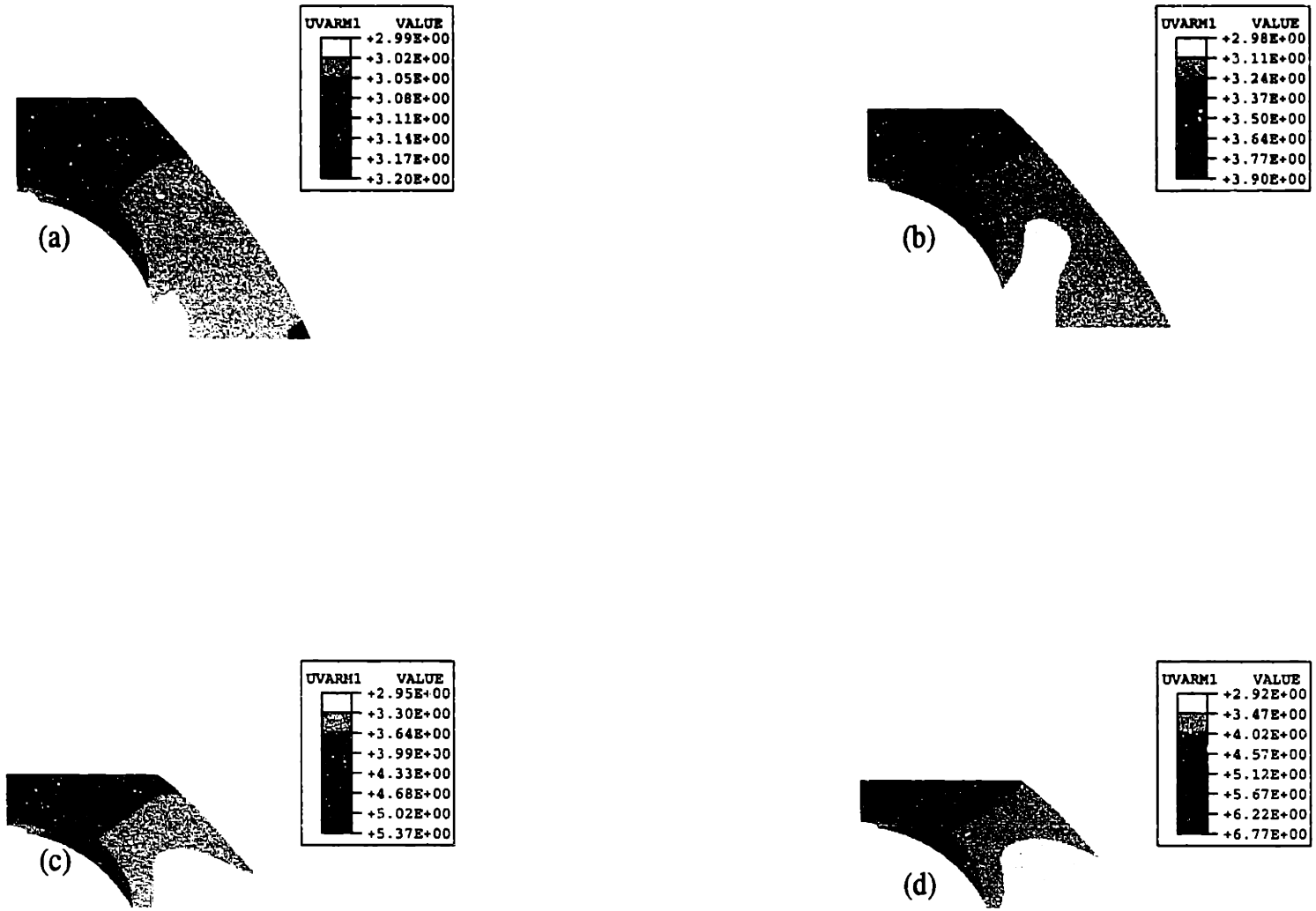

Figure 3.28: First Strain Invariant of V-BCC in Compression 15% Vf: (a) E_z=0.1, (b) E_z=0.2, (c) E_z=0.3, (d) E_z=0.36

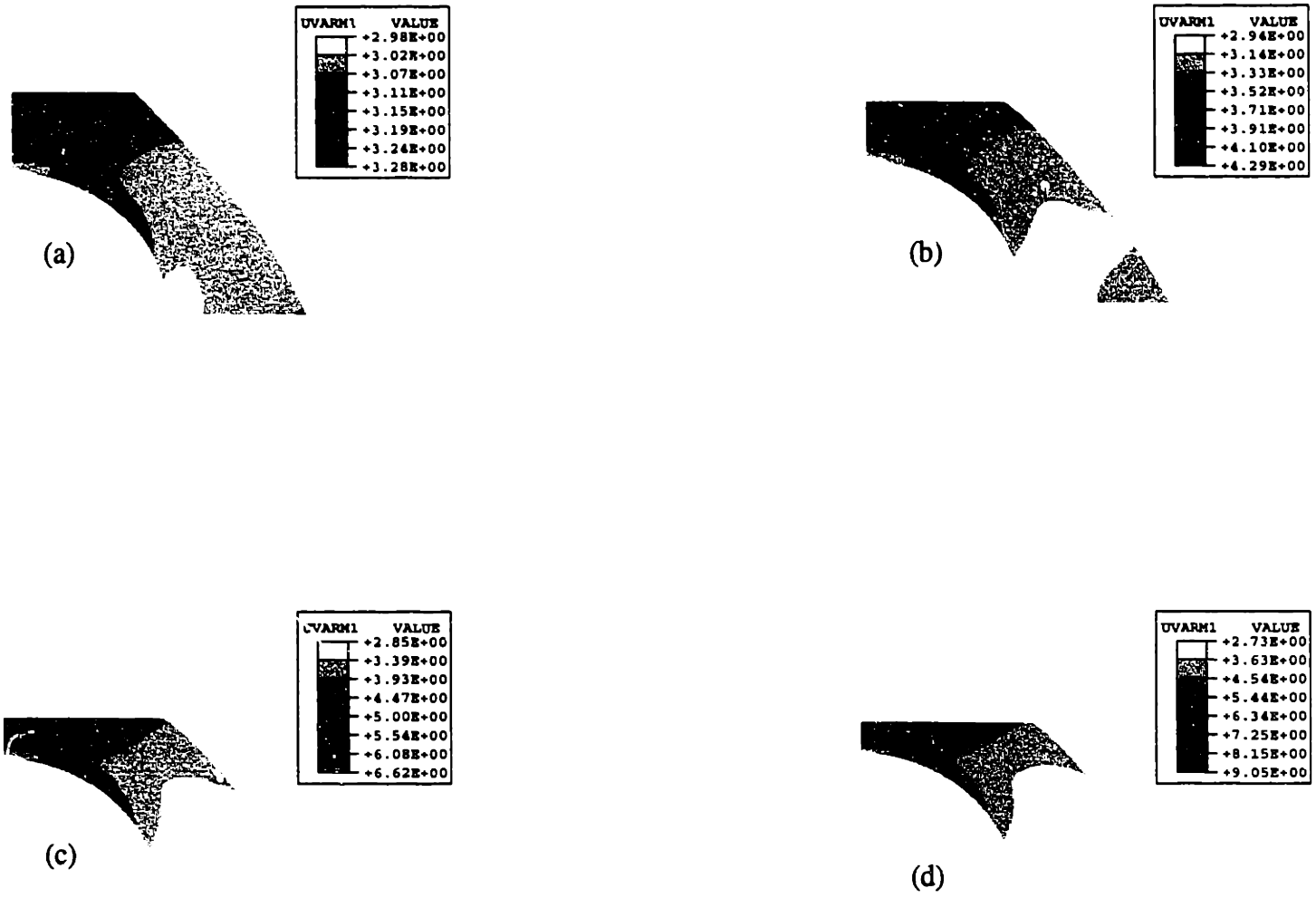

Figure 3.29: First Strain Invariant of V-BCC in Compression 20% Vf: (a) E_z=0.1, (b) E_z=0.2, (c) E_z=0.3, (d) E_z=0.36

3.2.7 Axial Stress Contour

Contour stress plots are shown for 10%, 15% and 20% volume fractions in Figures 3.30 through 3.32 respectively. Figure 3.30 illustrates the local axial stresses of the matrix material as the mesh evolves from an applied macroscopic compressive axial strain of E_z=-0.1 to E_z=-0.36. The local stresses are largest directly above the filler particle since loading is in the axial direction. The negative value of stress implies compression thus the greater the magnitude the greater the stress. These stresses are approximately 3 times greater than the macroscopic cell stress as seen in Section 3.2.2. The local stresses are smallest to the right of the particle and are about 1/3 the value of the macroscopic stress. It can also be seen that the local stress is approximately equal to the macroscopic stress at the vertical center of the contour plots. Figures 3.31 and 3.32 depict similar localized stress behavior with even greater local stress values due to the increased volume fraction of filler particles.

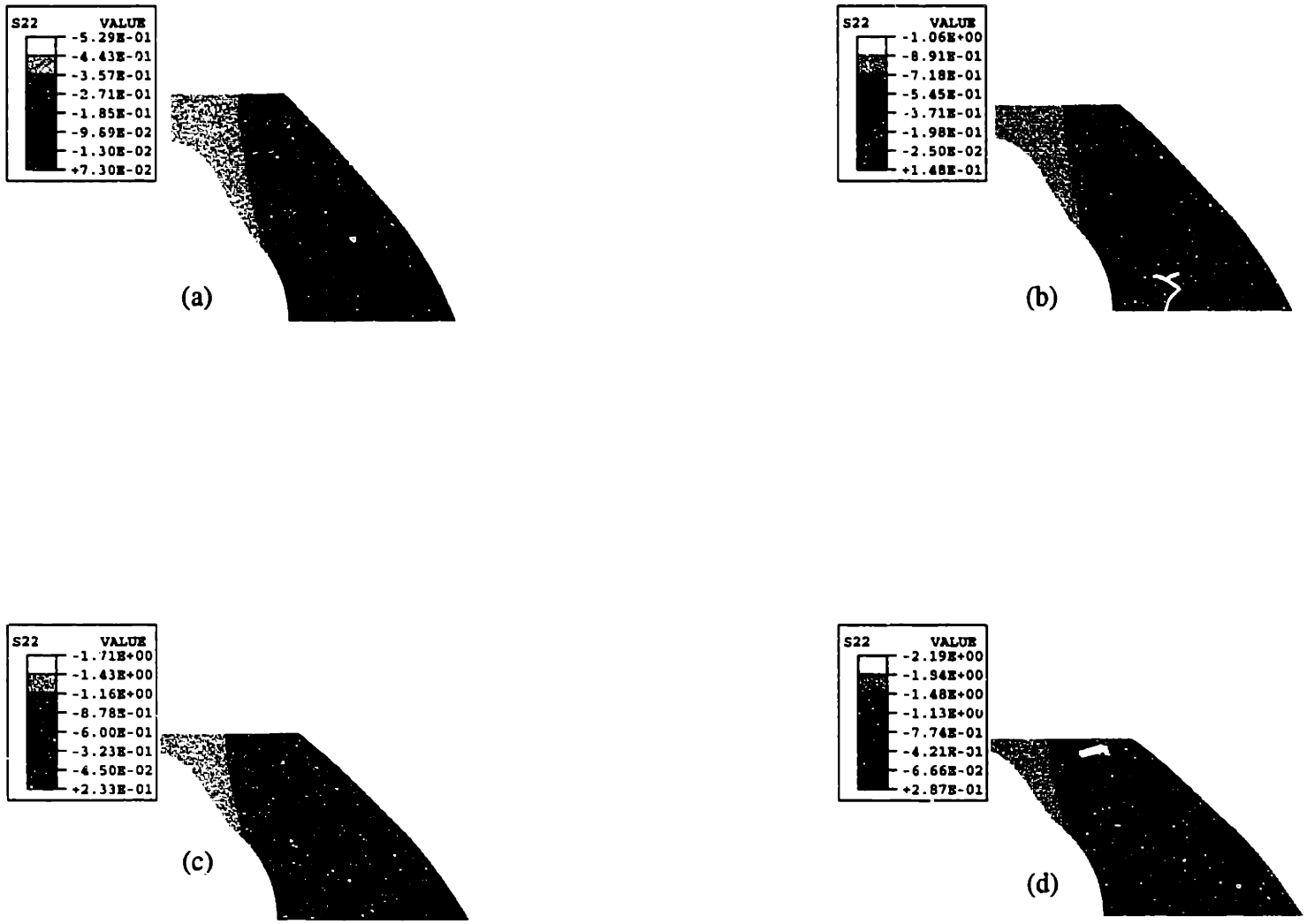

Figure 3.30: Compressive Axial Stress of V-BCC for 10% Vf: (a) E_z=0.1, (b) E_z=0.2, (c) E_z=0.3, (d) E_z=0.36

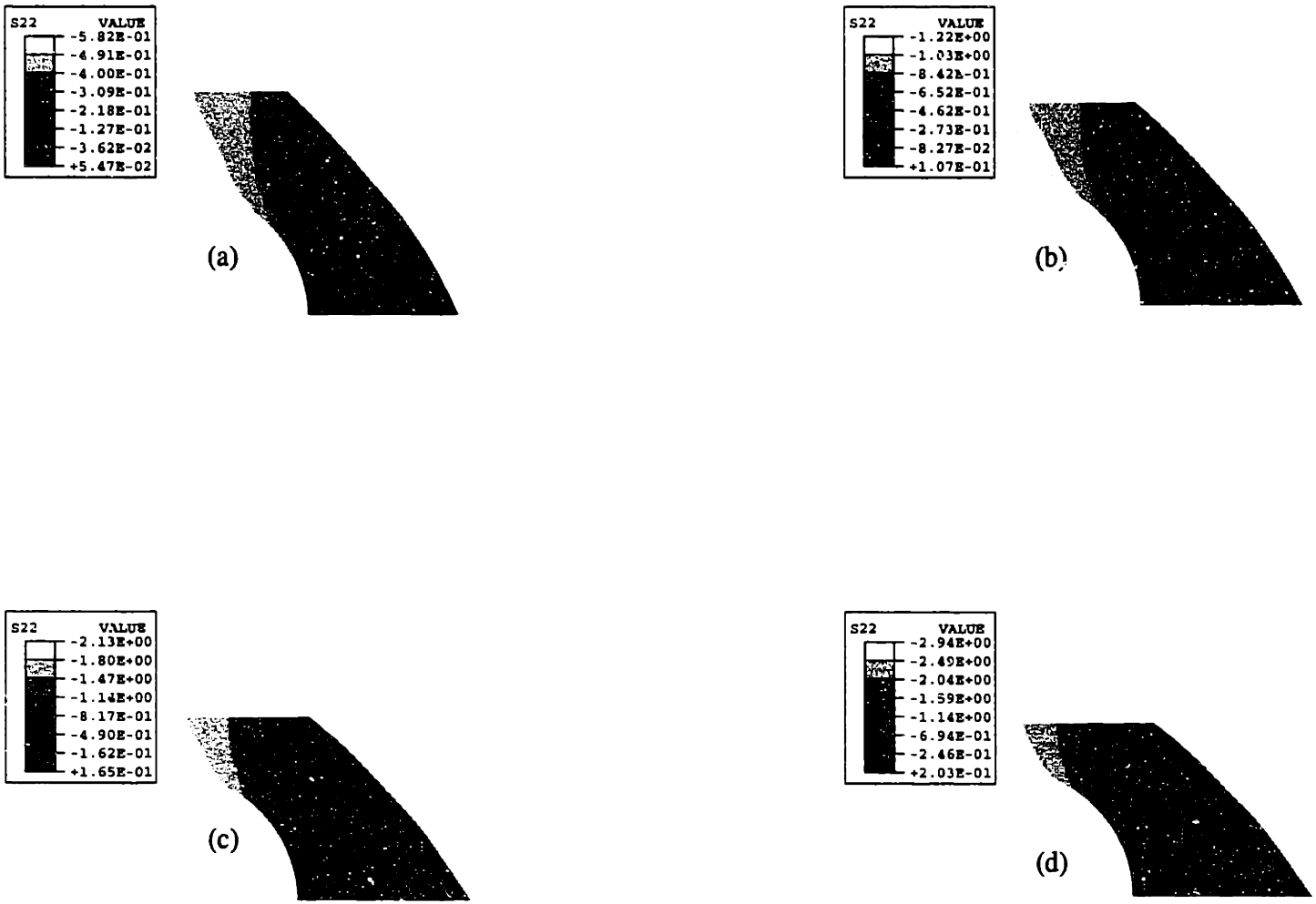

Figure 3.31: Compressive Axial Stress of V-BCC for 15% Vf: (a) E_z=0.1, (b) E_z=0.2, (c) E_z=0.3, (d) E_z=0.36

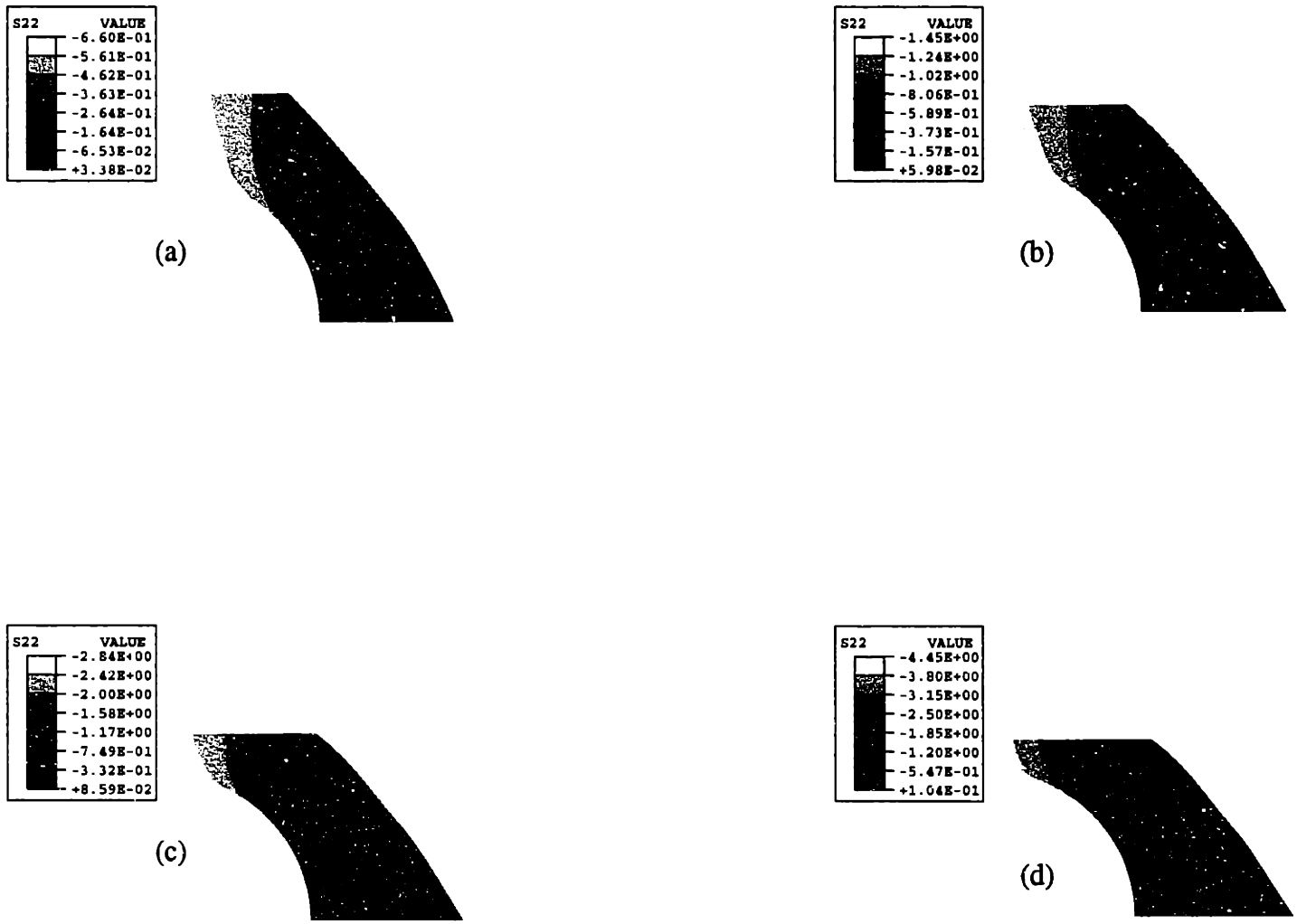

Figure 3.32: Compressive Axial Stress of V-BCC for 20% Vf: (a) E_z=0.1, (b) E_z=0.2, (c) E_z=0.3, (d) E_z=0.36

4. Conclusions and Recommendations

4.1 Closing Remarks

The effect of the filler particles on the elastomer results in various levels of strain, stress, and stretch distributions locally thoughout the matrix material. The presence of the rigid particles acts to amplify the stretches incurred in the matrix material as compared to the applied stretches as shown by contours of strain and stretch in the matrix; the local amplification results in the stiffer macroscopic behavior as evidenced in the computed stress-strain curves and tangent modulus for the composite materials. Simulations show increase in stiffness with increasing filler content as one would expect and as found experimentally. As volume fractions = 0.20 is reached in the elastomer, the stress-strain curve becomes rather dramatically stiffer as also seen in experiments by Bergstrom and Boyce [2]. This increase in stiffness with added amounts of filler particles is shown to be due to the rather thin ligament of matrix material that exists between particles at the high volume fractions where a small amount of matrix material must accommodate large amounts of stretch.

4.2 Future Work

This thesis only studies the effect of various volume fractions of filler particles on the mechanical properties of the filled elastomer. Further study should also be conducted to find the effects of the strain rate loading on the filled elastomers since the material deformation is time dependent. In addition, due to the Mullins effect (material softening from loading and unloading of the material), hysteresis should be studied using the V-BCC two-dimensional axisymmetric model at various volume fractions of filler particles and compared to the experiments of Bergstrom and Boyce [2].

Appendix A

The eight chain model is used such that in response to any deformation a principal stretch frame exists and the chains in that reference frame will undergo stretches describable by the principal values of stretch, λ_1, λ_2, λ_3 [1]. See Figure 2.4 for the eight chain model in a stretched configuration. The unstretched chains are of length

$$r_0 = \sqrt{N}l \tag{A.1}$$

where N is the number of rigid links of equal length l. The limiting extensibility is thus defined as final length divided by initial length $\lambda_L = \sqrt{N}$. The eight chain model is allowed expansion along each principal direction subject only to incompressibility which can be expressed as

$$\lambda_1\lambda_2\lambda_3 = 1. \tag{A.2}$$

The stretch on each chain in the network is given, in terms of the applied stretches, by

$$\lambda_{chain} = \sqrt{\frac{1}{3}(\lambda_1^2 + \lambda_2^2 + \lambda_3^2)}. \tag{A.3}$$

References

[1] Arruda,E.M., Boyce, M.C., (1992), "A Three-Dimensional Constitutive Model For the Large Stretch Behavior of Rubber Elastic Materials", *Journal of the Mechanical Physics of Solids, Vol.41.No. 2.*, 1993.

[2] Bergstrom, J.S., Boyce, M.C., "Mechanical Behavior of Particle Filled Elastomers", to appear in Rubber Chemistry and Technology, 1999.

[3] Bergstrom, J.S., Boyce, M.C., (1997), "Constitutive Modeling of the Large Strain Time-Dependent Behavior of Elastomers", J. Mech. Phys. Solids, Vol. 46, No. 5, pp. 931-954, 1998.

[4] Boyce, M.C., Socrate, S., (1999), "Micromechanics of Toughened Polycarbonate", to appear in Journal of the Mechanics of Physics of Solids, 1999.